5.1 INTRODUCTION

The conglomerates in the Ransi Member are poorly sorted with class ranging from granule to cobble size and are generally clast-supported. The clasts are mainly angular to subrounded (except for the Pelungau outcrop where they are all rounded to well rounded) and composed of rhyolitic rocks (Plate 5.15), quartzite (Plate 5.1), chert (Plate 5.6; 5.7) and some schist (Plate 5.14). The Ransi Member conglomerate consists almost exclusively of quartz and rock fragments. The quartz grains include low grade metamorphic vein quartz and chert. The clasts are poorly sorted and range from 1cm up to 50cm in size. The matrix of the conglomerates is composed of medium to very coarse sand with very little clay present. The conglomerate overlies with angular unconformity the Eocene marine turbiditic Belaga Formation (Fig. 4.3; 4.4).

The Ransi Member conglomerates are epiclastic conglomerates with clasts generated by the breakdown of older rocks of Belaga Formation through the processes of weathering and erosion. The clasts of these deposits range from sub-angular to rounded depending on the duration of transport and reworking, and durability of the clasts. Less durable clasts of shale and soft sandstone were commonly found in the Pelungau conglomerates and tend to be more rounded compared to the metasedimentary and quartzite clasts from the other exposures at Tutong Hill and the Hormat Pasifik Quarry.

The Ransi Member is situated in the lower part of the Tatau Formation. The absence of diagnostic fossils and maker beds correlation between the localities difficult. Lithological beds as markers are limited in their use for correlation between localities

because the sequences are highly variable and also of limited lateral extent in the near-shore high energy environment.

5.2 PETROGRAPHY OF THE RANSI MEMBER

Ransi Hill Conglomerate

The Ransi Hill conglomerate contains quartzite, chert and minor sandstone clasts. Rare thin shale beds are present between the conglomerate and sandstone beds. The conglomerate beds are matrix-supported (Fig. 5.1). The sub-angular to sub-rounded clasts are very poorly sorted and range from 5cm to over 20cm in size. The sandy matrix is about 30%. The conglomerate overlies with angular unconformity the turbiditic Eocene Belaga Formation from which *Bathysiphon sp.* was recovered (Fig. 4.14).

Gravel-size particles make up the framework grains of the conglomerates. They consists of metamorphic (quartzite and schist clasts) and sedimentary clasts (chert) with only some igneous clasts suggesting a predominantly metamorphic and sedimentary source (Fig5.1). The composition of the clasts of the Ransi Hill conglomerate is quartzite (50%), chert (27.8%), shale (5.6%), sandstone (5.6%), rhyolitic (11%) and rare schist fragments (Table 5.1).

The composition of clasts in conglomerate deposits can be a function of sorting (Boggs, 1969). Some parent rocks break down to yield a wide range clasts of different

sizes, whereas others break down to smaller clasts of the same size (Pettijohn, 1975). Less durable fragments such as shale clasts tend to break into smaller sizes and become more rounded during transport whereas more durable fragments such as chert, metaquartzite and resistant igneous fragments will tend to form relatively bigger grains and are less rounded (Boggs, 1992).

The matrix of the conglomerates is composed mainly of coarse sand particles that fill the interstitial spaces between the granule to cobble-size clasts (Fig. 5.3). It consists of a range of sand-size quartz and fine rock fragments. The matrix is generally cemented with quartz and hematite (iron oxide).

The clasts in this conglomerate are made up of 76.4% stable clasts such as quartzite, chert and vein quartz. They are polymict conglomerates with clasts of mixed lithology (Fig. 5.1). Most of the clasts in the conglomerates is quartzite of metamorphic origin. The quartz grains exhibit a foliation pattern and undulatory extinction when observed under thin section (See Plate 5.1).

The conglomerate beds in Ransi Hill consist of coarse clasts up to cobble size and deposits with more sand matrix but less than framework clasts. Pebble to cobble size particles are poorly to moderately rounded indicating comparatively short distances of transport (Seiders & Blome, 1988; Boggs 1992). The massive metaquartzite clasts are more angular. The conglomerate beds are normally graded.

Clast Type	Size (cm)	Roundness
Quartzite	20	sub-rounded
	20	sub-rounded
	15	sub-angular
	10	sub-angular
	10	sub-angular
	7	sub-angular
	6	sub-angular
	5	sub-rounded
	5	sub-angular
Chert	4	sub-angular
	3	sub-angular
	3	sub-angular
	2	sub-angular
	2	rounded
Igneous	3	sub-angular
	3	sub-angular
Shale	5	rounded

Table 5.1 Clasts size, composition and its roundness of the Ransi Hill conglomerate.

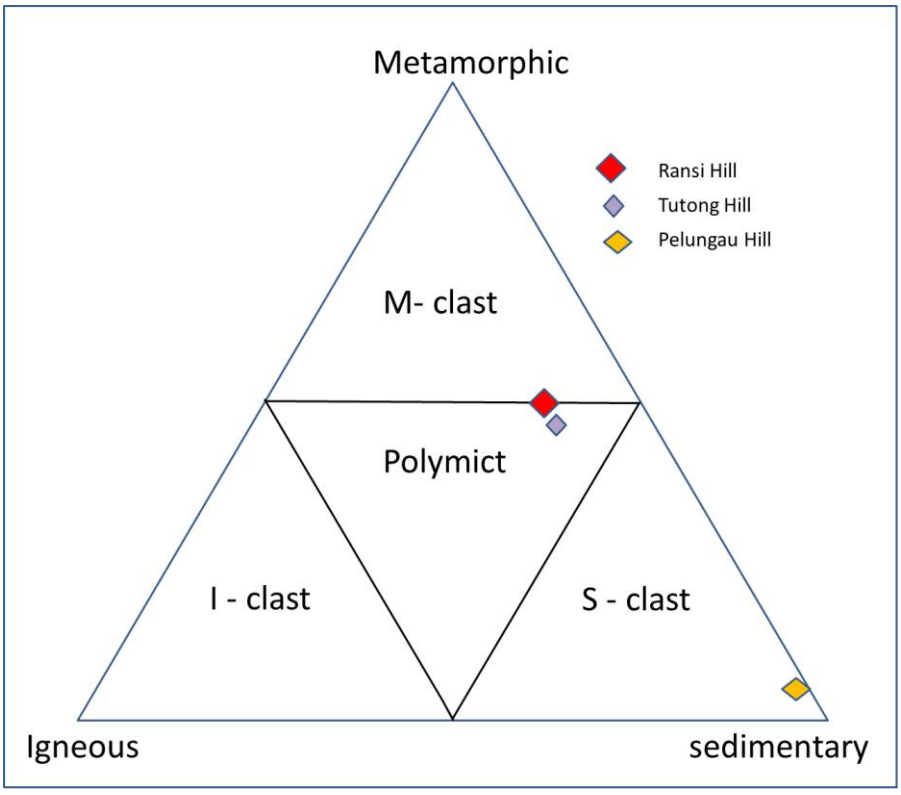

Fig. 5.1 Conglomerate clasts provenance plotted in Boggs (1992) classification chart.

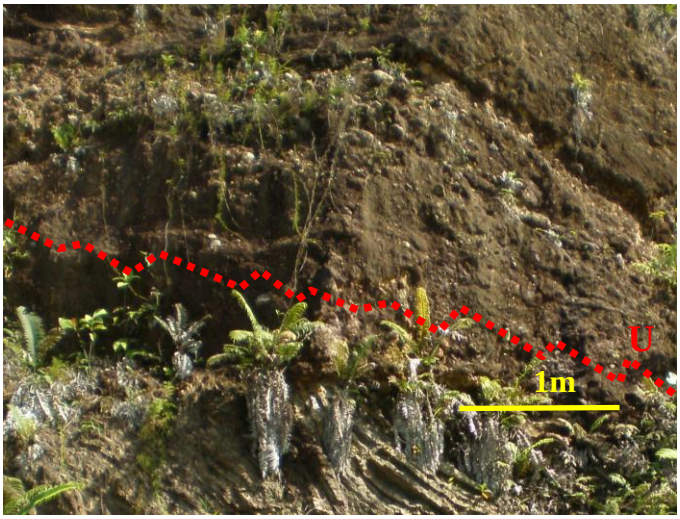

Fig. 5.2 Thick graded Ransi Member conglomerate beds sitting on top of tightly folded Bawang Member turbidite at locality L7, Ransi Hill.

Fig. 5.3 Cobble sized clasts in Ransi Hill conglomerate bed (scale is in 5cm).

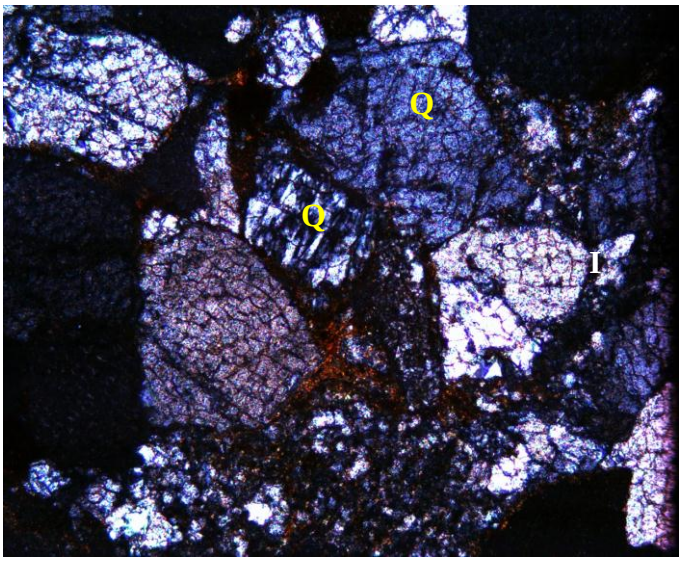

Plate 5.1 Thin section of locality L4 showing metamorphic quartz (Q) with undulatory extinction (cracking in quartz grains are an artifact of thin-sectioning).

Tutong Hill

Conglomerate

The Tutong Hill conglomerate consists of chert, quartzite, sandstone fragments and minor granitic fragments. Thin shale and pebbly sandstone beds gradually become more abundant in the upper part of the sequence. The conglomerate is clast-supported (Fig. 5.4). The clasts are very poorly sorted and the grains are subangular to rounded with clasts that range from 2cm to over 15cm. Soft clasts of sandstone and shale are more rounded compared to quartzite and chert (Fig. 5.5). The percentage of the matrix is about 35% and matrix is generally made up of medium to fine sand (Fig. 5.6). The conglomerate overlies with angular unconformity the turbiditic Eocene Belaga Formation.

The composition of the clasts of the Tutong Hill conglomerate beds is mainly of quartzite, metasediment, chert and igneous fragments. The chert and quartzite clasts tend to be sub-angular to sub-rounded, whereas the shale and sandstone clasts are more rounded (Table 5.2). This is due to their different durabilities with the more resistant clasts tending to be more angular and bigger compared to the less durable shale clasts (Boggs, 1992).

The matrix of the Tutong Hill conglomerate is mainly of medium to fine sized sand. The matrix is cemented by quartz and secondary iron oxide. The conglomerate beds consist of sub-rounded clasts ranging from 1cm to 8cm across. The beds are normally graded (Fig. 5.4). The geometry of sub-rounded clasts suggests that they had

been transported quite far from the source area and deposited within a high energy fluvial environment (Seiders & Blome, 1988). Sedimentary structures and paleocurrents suggest that conglomerates are fluvial channel deposits.

It is a polymict conglomerate of mixed origin with about 70% quartzite and chert clasts and 30% of clay clasts and matrix.. The abundance of polycrystalline quartz suggests a low-grade metamorphic origin (Table 5.4 & Fig. 5.10).

Clast Type	Size (cm)	Roundness
Quartzite	9	sub-angular
	6	sub-angular
	4	sub-angular
	4	sub-angular
	4	rounded
	3	sub-rounded
	2	sub-angular
	2	sub-angular
Chert	3	sub-angular
	3	sub-rounded
	2	sub-angular
	2	sub-rounded
	2	sub-rounded
Igneous	3	sub-angular
	3	sub-angular
Shale	3	sub-rounded
	3	rounded

Table 5.2 Clasts size, composition and its roundness of the Tutong Hill Conglomerate.

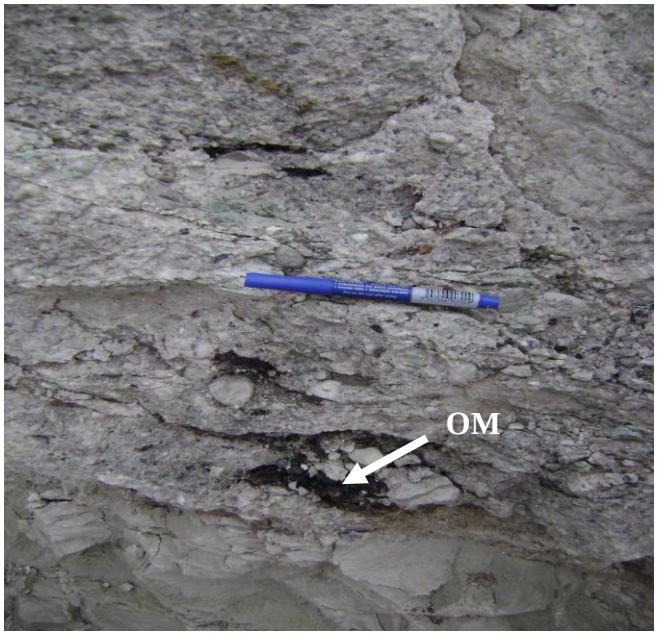

Fig. 5.4 Graded conglomerate bed with pebble-sized clasts and organic matter (OM) at locality L2, Tutong Hill.

Fig. 5.5 Sub-angular to sub-rounded clasts in cut conglomerate hand specimen from locality L1, Tutong Hill. Matrix is cemented with hematite minerals.

Fig. 5.6 Clast supported thick conglomerate beds at locality L2, Tutong Hill.

Sandstone Petrology

The Tutong Hill section overlies an angular unconformity above the Eocene low grade metamorphosed shaly Belaga Formation. The beds generally dip 30° to 40° northwestward. The pebbly sandstone beds are normal graded fining upward in general (Fig. 5.7; 5.8)

The petrographic characteristic of the sandstone from facies F2 of the Ransi Member throughout the section of the Tutong Hill is similar. All are quartz-rich pebbly sandstone dominated by quartz, i.e 29% - 50%, some rock fragments (9% - 29%) and very little highly weathered feldspar mineral (less than 1%) (Table 5.3). Some of the feldspars are hard to identify because they are highly altered to clay. The feldspar grains showed very weak twinning and low relief with abundant dirty inclusions in them (probably clay mineral as alteration products).

The Tutong section sandstones are sublitharenites to litharenites according to the QFL (Quartz-Feldspar-Lithic fragment) plots with the abundance of quartz and rock fragments and very little or no feldspars (Fig. 5.9).

Most of the sandstone specimens are very poorly sorted with a wide range of the grain size distributions, the grains are subangular and only some relatively soft sedimentary clasts are subrounded (See table 5.4 & Fig. 5.8; 5.11). The sizes of the sands grains range from fine to very coarse, although most are medium to very coarse. The percentage of the matrix is variable, ranging from 1% up to 8%, with most values between 3% and 5%. Some detrital grains were deformed to a pseudomatrix (Plate 5.2). Cement ranges from 0.4% to 2.5%, but are more commonly 1% to 2% (Fig. 5.10). The

most abundant cement in the sandstone consists of silica (Plate 5.3). Some secondary overgrowths of quartz are present.

The grain size plots of the samples collected from Tutong Hill show the distribution of sizes throughout the whole logged section. Sample TL1 (Fig. 5.11) falls in the range of medium to very coarse sand, i.e. 0.45mm to 1.00mm and above. The positive skewness of the grain size distribution suggests a coarse grain bed. The sorting of the bed is very poor (Table 5.5). Sample TL2 from overlying bed shows a bimodal distribution of grain sizes of mostly medium to very coarse sand (0.25mm to more than 1mm) (Fig. 5.11). Sample TL3 shows a relatively more even distribution with most grains in the range of coarse to very coarse sand (0.65mm to more than 1mm). The fine to medium grains made up of 5.5% of the sandstone (Fig. 5.11). The sorting of the TL3 sandstone is extremely poor with the standard deviation of grain size of as high as 16.32 (Table 5.5). Sample TL4 shows that most of the grain size is from coarse grain to very coarse grain (0.85mm to more than 1.00mm). The sorting of the sediment is extreme poorly sorted with a standard deviation of 17.34 (Table 5.5). Sample TL5 shows bimodal grain size distribution between coarse sand (0.45mm to 0.85mm) sand and very coarse sand (more than 1.00mm) coarse sand (Fig. 5.11). Sample TL6 shows a relatively more normal distribution, with grain sizes increasing gradually from medium to more than very coarse sand (Fig. 5.11). The sediment is very poorly sorted according to the standard deviation of grain size. The grain size distribution of TL7 shows that the sandstone is normally distributed where most of the grain size is from medium sand to coarse sand (0.25mm to 0.85mm) (Fig. 5.11). The TL7 bed is very poorly sorted with a standard deviation of 12.32 (Table 5.5). TL8 is a very coarse sandstone with most of the grains of normally very coarse sand (more than 1.mm) (Fig. 5.11). The bed is extremely

poorly sorted with a standard deviation of 26.85. Sample TL9 shows a wide distribution of the grain size from medium to very coarse sand (0.45mm to more than 1mm) with a positive skewed coarser distribution (Fig. 5.11). The bed is very poorly sorted with a standard deviation of 11.03. The sample TL10 shows random distribution with a grain size is range from medium to very coarse sand (0.45mm to 1mm) (Fig. 5.11). The standard deviation suggests extremely poor sorting (16.10) of the sandstone (Table 5.5).

The framework quartz grains have mainly undulatory strained extinction under cross-nicol and are mostly polycrystalline quartz (24% to 50%) (Table 5.4). Monocrystalline quartz only makes up 7% to 16% of the sandstone samples (Plate 5.4). The quartz grains are subangular to subrounded in shape with various grain sizes that suggests poor sorting. Quartz overgrowths are common (Plate 5.3). Mica inclusions are found within some quartz grains indicating derivation from a similar source to the rocks at Tatau Hill and Hormat Pasifik Quarry (Plate 5.5). Metamorphic quartz with sutured boundaries are common. Concave-convex contacts of the quartz grains as a result of pressure solution were also observed between some grains (El-Ghali et al., 2009). Some pseudomatrix created as clay was squeeze in between some grains by secondary quartz growth during cementation (See Plate 5.2) (EL-Ghali et al., 2009).

The presence of radiolarian chert is variable in the sandstones. The original opaline silica in the radiolaria had been replaced by later microcrystalline quartz (Plate 5.6) (Adams et al., 1984; Scholle, 1979). Radial fibrous chacedonic quartz occurs as pore fillings of radiolaria in the chert (Plate 5.7).

Rock fragments are significant constituents of the sandstones. A few types of rock fragments were identified from the specimens. The most common type is metamorphic rock fragments. The schistose fragments are of micro quartz with preferential alignment of elongated grains (Plate 5.4). The spherulitic texture of the igneous rhyolitic fragments similar to the Piring Hill dyke rock is found in some igneous fragments (Plate 5.8). Clay-rich clasts of weathered argillaceous rocks are present in the form of aggregates of sericite and phyllosilicates that filled the pore spaces (Plate 5.3).

Highly altered weathered feldspar grains by saussuritization, calcitization, kaolinization and sericitization were produced by weathering in humid environments. Most grains are completely altered making identification of the original grains difficult.

Other minerals such as pyrite are commonly present in some of in the sandstones. Iron coated sedimentary quartz grains are probably due to iron staining during weathering (Plate 5.9). There is no heavy minerals detected in the sandstone.

Fig. 5.7 Graded bed of pebbly sandstone from facies F1Ransi Member, locality L1, Tutong Hill.

Fig. 5.8 Hand specimen of Ransi Member graded pebbly sandstone from facies F2, locality L2, Tutong Hill.

Mineral	TL1		TL2		TL3		TL4		TL5		TL6	
		%		%		%		%		%		%
quartz total (quartz & chert)	318	80.3	269	74.3	324	79.6	379	88.6	254	74.1	318	72.4
Rock fragment	78	19.7	93	25.7	76	18.7	43	10.0	83	24.2	121	27.6
Feldspars	0	0.0	0	0.0	7	1.7	6	1.4	6	1.7	0	0.0
TOTAL	396	100.0	362	100.0	407	100.0	428	100.0	343	100.0	439	100.0

Mineral	TL7		TL8		TL9		TL10	
		%		%		%		%
quartz total (quartz & chert)	226	66.3	369	81.5	324	71.1	395	80.8
Rock fragment	110	32.3	84	18.5	128	28.1	94	19.2
Feldspars	5	1.5	0	0.0	4	0.9	0	0.0
		0.0						
TOTAL	341	100.0	453	100.0	456	100.0	489	100.0

Table 5.3 Mineral compositions of pebbly sandstone and sandstone samples from Tutong Hill outcrops.

Quartz type (%)	TL1	TL2	TL3	TL4	TL5	TL6	TL7	TL8	TL9	TL10
Polycrystalline,<3	3.8	9.4	14.3	11.1	4	6.7	11.5	4.2	3.6	7.1
polycrystalline, >3	34.6	40.6	21.4	25.9	20	33.3	23.1	29.2	28.6	28.6
undulatory quartz	46.2	34.4	50	55.6	64	46.7	53.8	58.3	60.7	53.6
monocrystalline	15.4	15.6	14.3	7.4	12	13.3	11.5	8.3	7.1	10.7

Table 5.4 Quartz provenance analysis based on Framework quartz grains types in thin sections of samples.

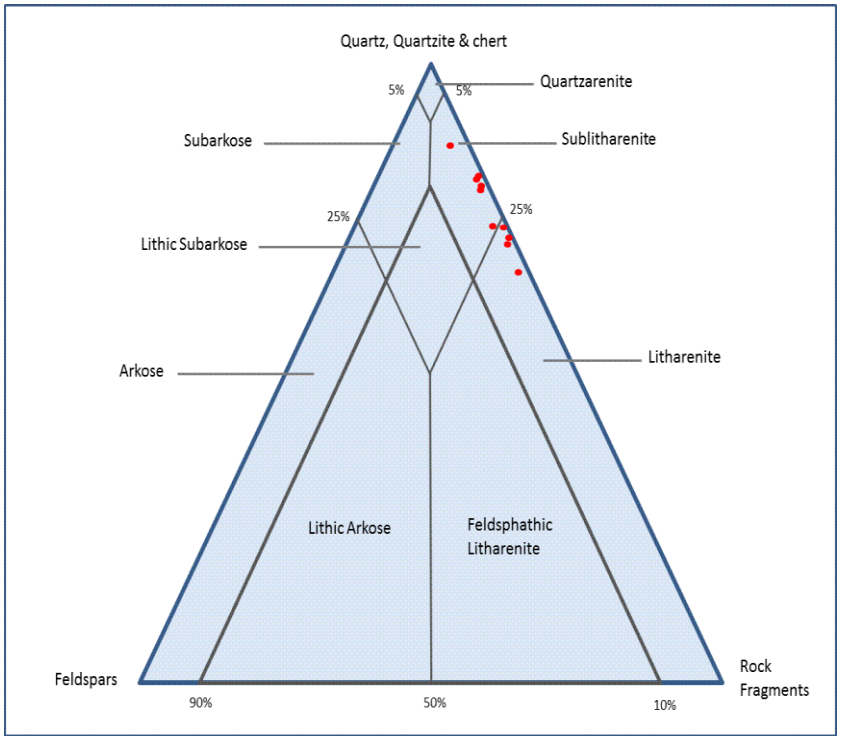

Fig. 5.9 Tutong Hill sandstones plotted in Mc Bride's (1963) classification chart.

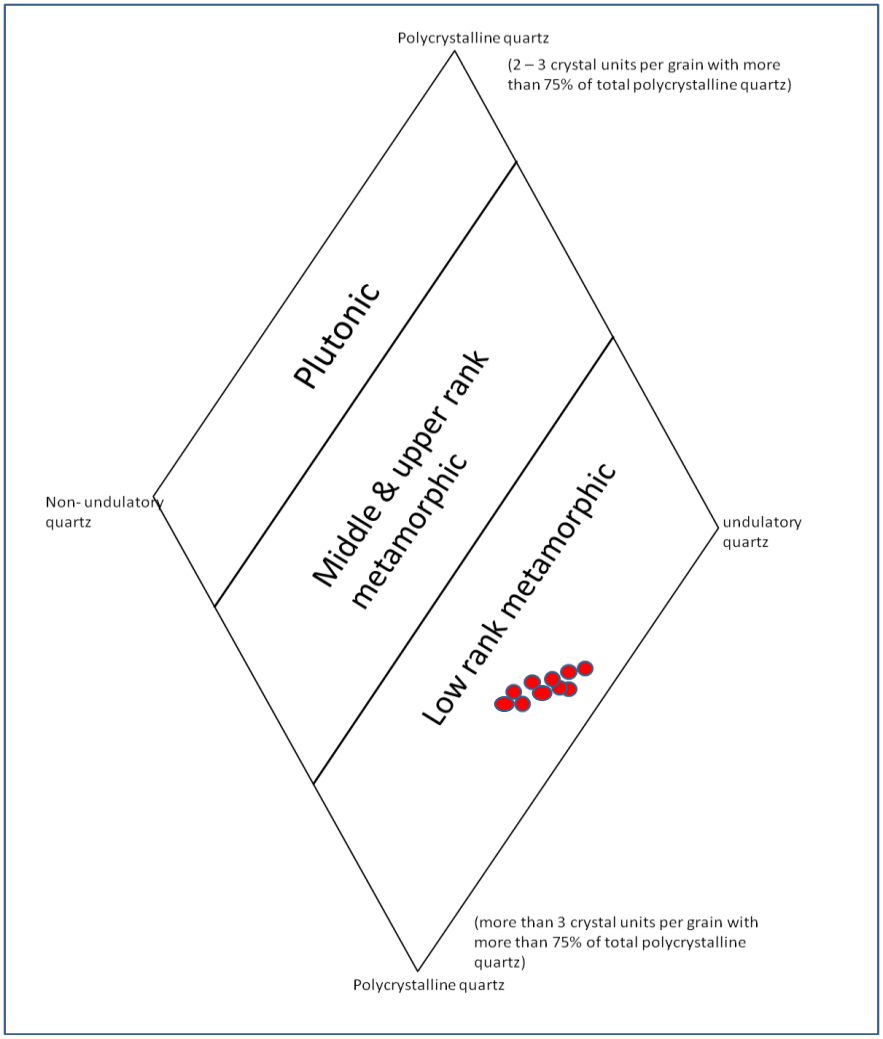

Fig. 5.10 Quartz grains provenance plotted on classification chart (Basu et al.,1975).

Grain Size (mm)	TL1		TL2		TL3		TL4		TL5		TL6	
		%		%		%		%		%		%
> 1.00	44	16.06	61	32.11	164	43.16	214	30.14	145	42.27	185	41.76
1.00-0.85	66	24.09	14	7.37	34	8.95	315	44.37	20	5.83	70	15.80
0.84 - 0.65	56	20.44	25	13.16	118	31.05	104	14.65	64	18.66	100	22.57
0.64 - 0.45	72	26.28	58	30.53	43	11.32	62	8.73	74	21.57	65	14.67
0.44 - 0.25	25	9.12	29	15.26	21	5.53	9	1.27	36	10.50	23	5.19
< 0.25	0	4.01	3	1.58	-		6	0.85	4	1.17	-	
TOTAL	274	100.00	190	100.00	380	100.00	710	100.00	343	100.00	443	100.00
varians		75.80		151.76		266.38		300.66		215.91		186.36
std. dev (Sorting)	(V. poor)	8.71	(V. poor)	12.32	(Ex. Poor)	16.32	(Ex. Poor)	17.34	(V. Poor)	14.69	(V. Poor)	13.65

Grain Size (mm)	TL7		TL8		TL9		TL10	
		%		%		%		%
> 1.00	-		304	66.52	160	34.12	-	
1.00-0.85	31	7.83	24	5.25	101	21.54	138	27.06
0.84 - 0.65	129	32.58	91	19.91	101	21.54	157	30.78
0.64 - 0.45	134	33.84	19	4.16	92	19.62	186	36.47
0.44 - 0.25	82	20.71	19	4.16	15	3.20	26	5.10
< 0.25	20	5.05	-		-		3	0.59
TOTAL	396	100.00	457	100.00	469	100.00	510	100.00
varians		147.48		720.92		121.60		259.07
std. dev (Sorting)	(V. poor)	13.43	(Ex. Poor)	26.85	(V. Poor)	11.03	(Ex. Poor)	16.10

Table 5.5 Grain size distribution of pebbly sandstone and sandstone samples from Tutong Hill.

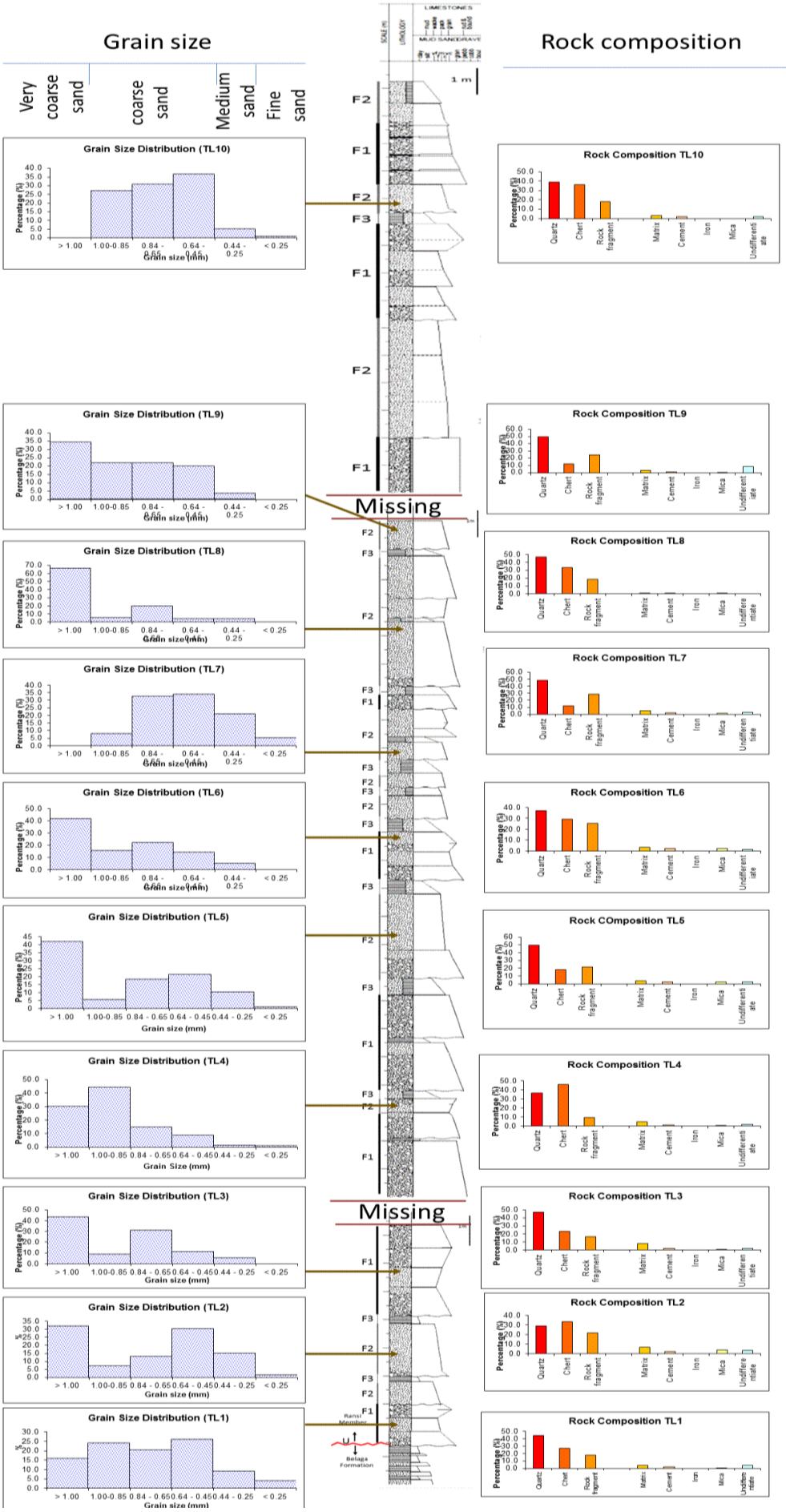

Fig. 5.11 Histogram of grain-size distribution and rock compositions of Tutong Hill (locality L1 & L2) sandstone from thin sections.

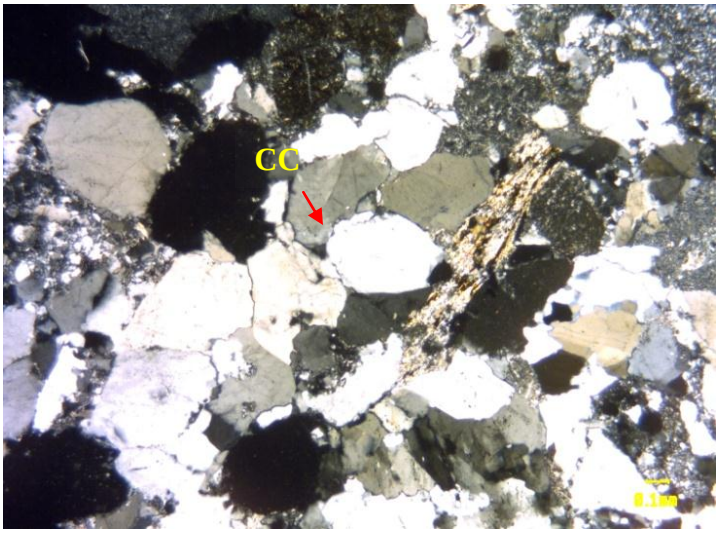

Plate 5.2 Thin section of TL 5 at locality L2, Tutong Hill showing concavo-convex (CC) contact of the quartz grains.

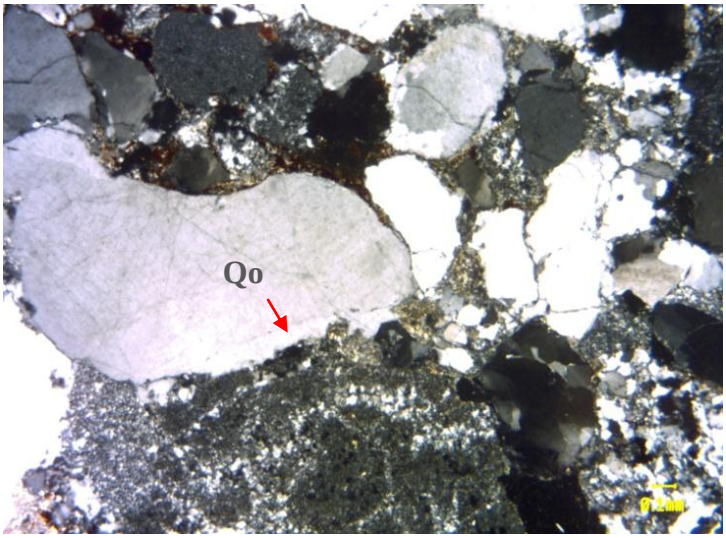

Plate 5.3 Thin section of TL 3, from locality L2, Tutong Hill showing secondary quartz growth (Qo).

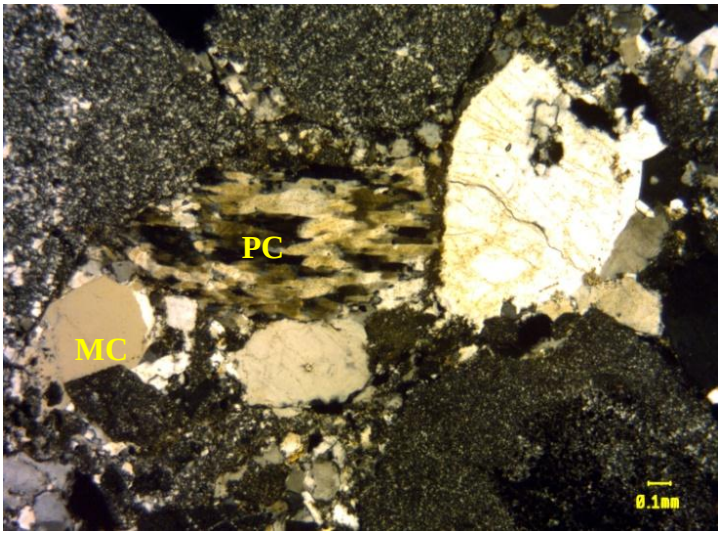

Plate 5.4 Thin section of TL 8 at locality L2, Tutong Hill showing metamorphic-origin polycrystalline quartz grain (PC) and monocrystalline quartz grain (MC).

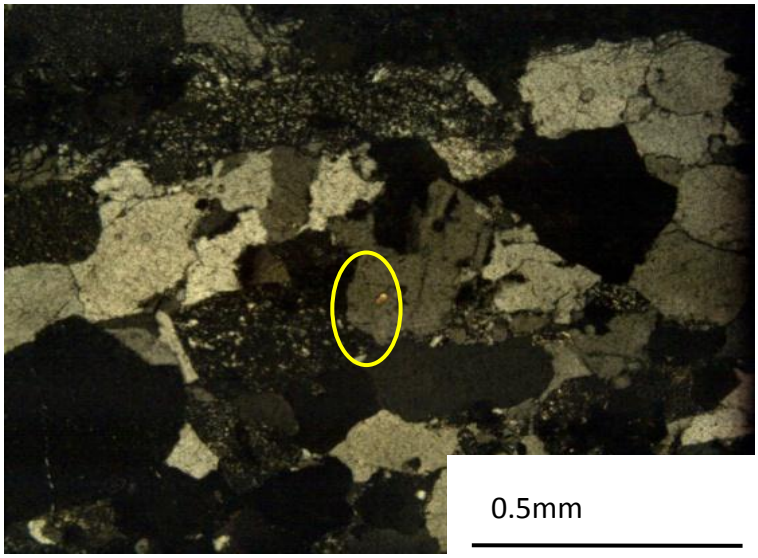

Plate 5.5 Thin section of TL 2 at locality L2, Tutong Hill showing mica inclusion within quartz grains (in yellow circle) used for characterizing quartz grain source provenance.

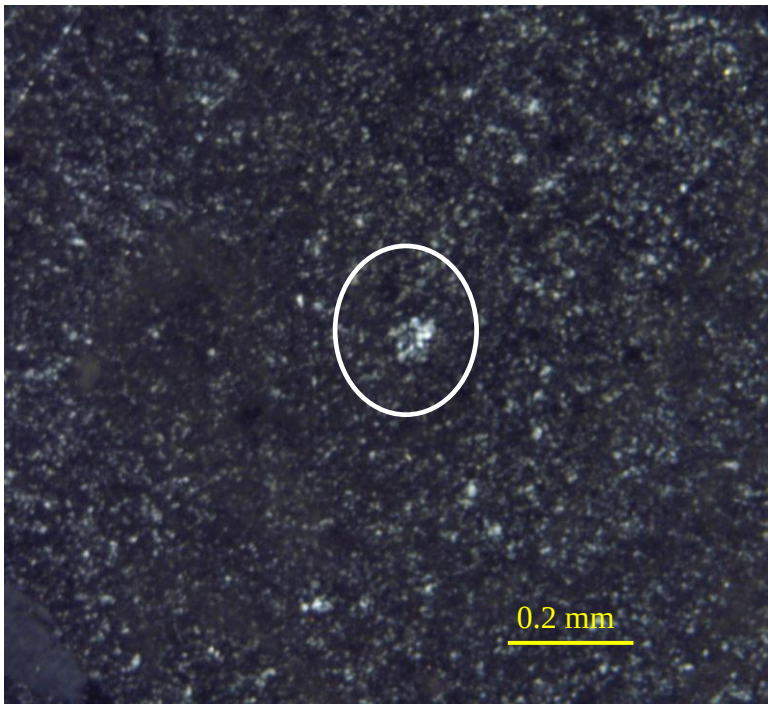

Plate 5.6 Thin section of TL 6 at locality L2, Tutong Hill showing radiolarian chert with microcrystalline quartz filling radiolarian (in white circle) .

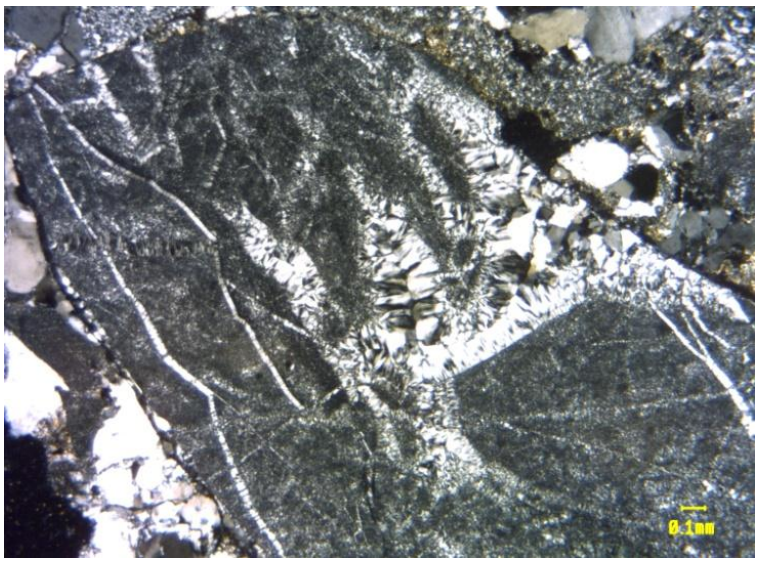

Plate 5.7 Thin section of Tl 5 at locality L2, Tutong Hill showing radial fibrous chacedonic quartz occuring as fracture fillings of radiolarian chert.

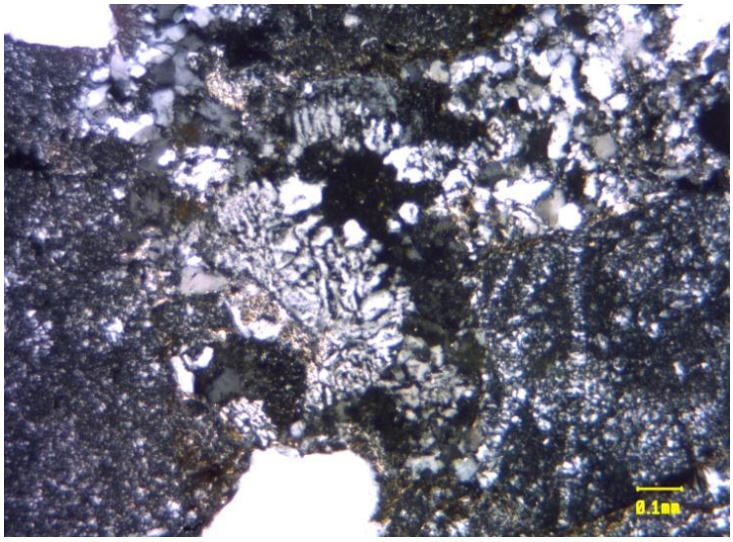

Plate 5.8 Thin section of TL 7 at locality L2, Tutong Hill showing rhyolitic igneous fragment with spherulitic texture similar to the Piring Hill rhyolite.

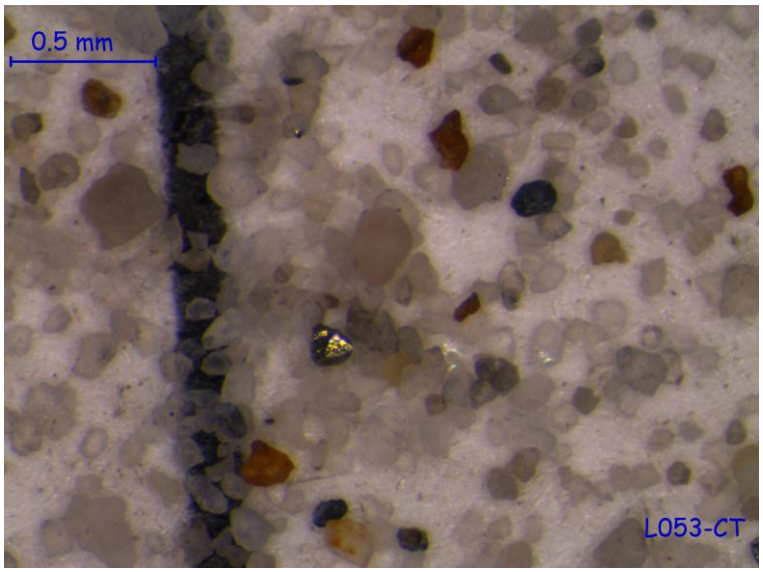

Plate 5.9 Pyrite (yellow) and iron (brown) grains found in the sandstone.

Tatau Hill

The petrographic characteristic of the sandstones throughout the section gradually changes from relatively coarse to medium grain upsection. Clay clasts are dominant at the upper section, whereas the lower section is rich in pebbly sandstone. In the lower section, the sandstone are quartz-rich with significant rock fragments (Fig. 5.15). Feldspar is rare throughout and all are highly altered. On the other hand, rock fragments and clay clasts dominate the upper section of Tatau Hill. Only the lower part of the outcrop was sampled as the upper part was highly weathered to loose soil.

The QFL plot (Table 5.6 & Fig. 5.13) of the Tatau Hill section shows that sandstones are sublitharenites with abundance of quartz (84% to 93%) and a fair amount of rock fragments (6% to 16%) with very little feldspar. Feldspar content is extremely low (0.2%) and negligible probably due to the high energy depositional environment and tropical climate that lead to the rapid alteration feldspars into clay.

The sandstone samples are extremely to very poorly sorted. The grains are subangular to subrounded with grain sizes ranging from medium to very coarse. Most of the samples consist of two groups of grain size distributions of either medium or very coarse grain (Table 5.8). The percentage of the matrix is 2% to 3%. Some detrital grains are formed as pseudomatrix squeezed and trap between grains (Fig. 5.14). Cement make up 1% to 2% of the sandstone and the most common cement is silica (quartz) with some iron oxide pore fillings (Fig. 5.11). Secondary overgrowth of quartz minerals is common in the samples (Plate 5.10).

The distribution of grain sizes of the samples collected from Tatau Hill are shown in Table 5.8. Sample TT1 from the lowest part of the logged section, shows a bimodal distribution high in coarse sand and very coarse sand, i.e. 0.46-0.65mm and more than 1mm (Fig. 5.14) with rare fine sand. The bed is extreme poorly sorted with standard deviation as high as 29. 07. Sample TT2 has a grain size distribution suggesting that generally the grain size is coarse grain to very coarse gain (0.46mm to more than 1mm), with a positively skewed plot suggesting that the coarse sandstone bed is extreme poorly sorted with a standard deviation of 18.30. Sample TT3 shows a bimodal distribution with grains high in the ranges of medium sand (0.25-0.45mm) and very coarse sand (more than 1mm). There is an absence of grains from 0.66-0.85mm. This bed is very poorly sorted with a standard deviation of 14. 49 compared to the older beds TT1 and TT2 below.

The framework quartz grains have mainly undulatory strained extinction and are mostly polycrystalline quartz (18% to 28%). Monocrystalline makes up only 7% to 9% of the sandstone (Table 5.7 & Fig. 5.12). The quartz grains are subangular to subrounded and very poorly sorted (Plate 5.11). Quartz overgrowth is common and some of the quartz contains mica inclusions (Plate 5.12). Concavo-convex contacts of the quartz grains are also common in the samples (Plate 5.11).

Radiolarian chert grains up to 40% are commonly found in the sandstone samples. The original opaline silica of the radiolaria had being replaced with micro quartz grains with rounded outlines (El-Ghali et al., 2009). Most of the chert grains are subangular to subrounded (Plate 5.13).

Rock fragments are frequently found in the sandstones (6% - 13%). Only a few types of rock fragments were identified. Metamorphic rock fragments with fine quartz aligned within a schistose texture is found in the samples (Plate 5.14). Rhyolite igneous fragment similar to that from Piring Hill were found in the sandstone samples (Plate 5.15). Clay clasts are also common in the sandstone.

Mineral	TT1		TT2		TT3	
		%		%		%
quartz total (quartz & chert)	581	93.3	517	86.2	364	84.5
Rock fragment	42	6.7	83	13.8	67	15.5
feldspars	0	0.0	0	0.0	0	0.0
						0.0
TOTAL	623		600	100.0	431	100.0

Table 5.6 Mineral composition of samples from Tatau Hill.

Quartz type (%)	TT1	TT2	TT3
Polycrystalline,<3	3.9	4.5	4.1
polycrystalline, >3	24.1	13.6	20.7
undulatory quartz	62.1	72.7	67.4
monocrystalline	6.9	9.1	7.8

Table 5.7 Composition of framework quartz grains of the samples from Tatau Hill.

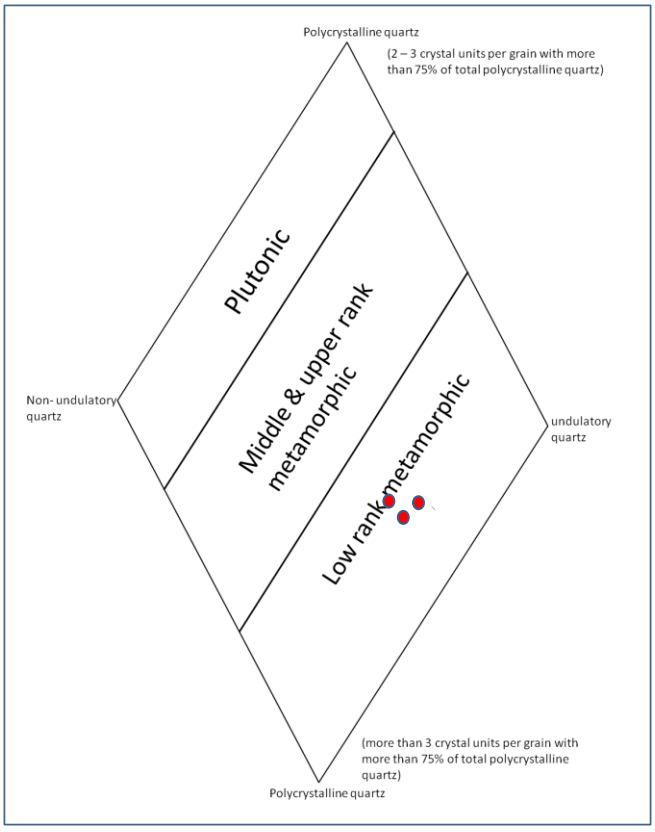

Fig. 5.12 Quartz grain provenance plotted in Basu et al. (1975) classification chart.

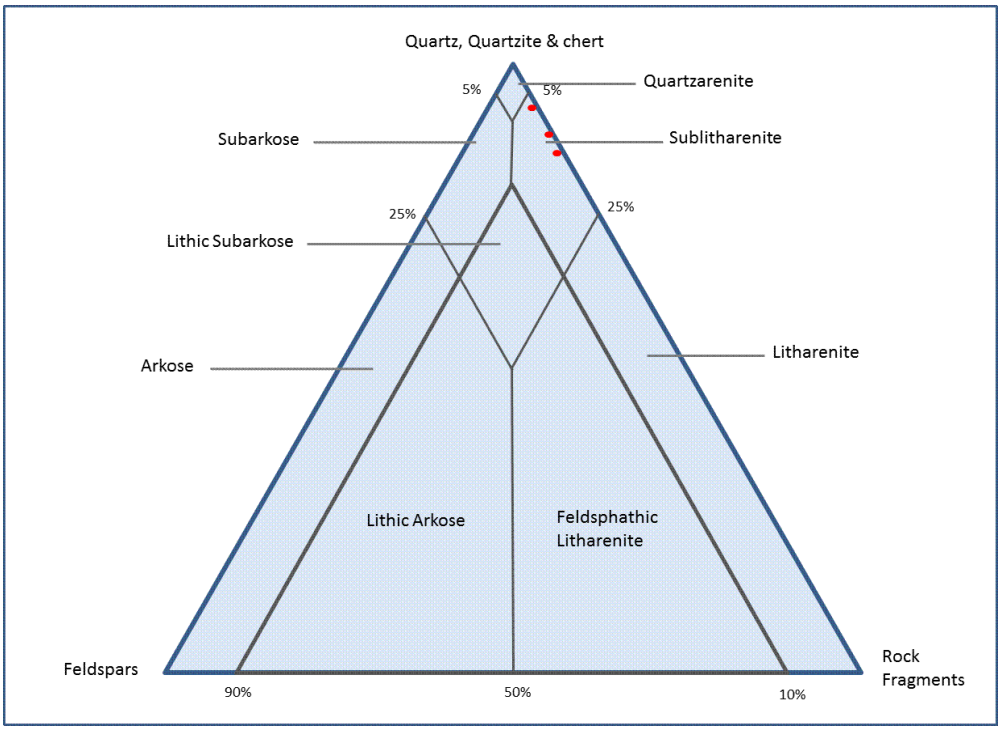

Fig. 5.13 Tatau Hill sandstones plotted on Mc. Bride's (1963) classification chart.

Grain Size (mm)	TT1		TT2		TT3	
		%		%		%
> 1.00	477	75.24	336	51.45	122	30.12
0.85-1.00	41	6.47	68	10.41	49	12.10
0.66-0.84	10	1.58	117	17.92		0.00
0.46-0.65	84	13.25	103	15.77	148	36.54
0.26-0.45	21	3.31	25	3.83	86	21.23
< 0.25	1	0.16	4	0.61	-	-
TOTAL	634	100.00	132	100.00	234	100.00
Varians		844.94		334.85		210.03
Std. Dev. (Sorting)	(Ex. Poor)	29.07	(Ex. Poor)	18.30	(V. Poor)	14.49

Table 5.8 Grain size distribution of the pebbly sandstone and sandstone samples from Tatau Hill.

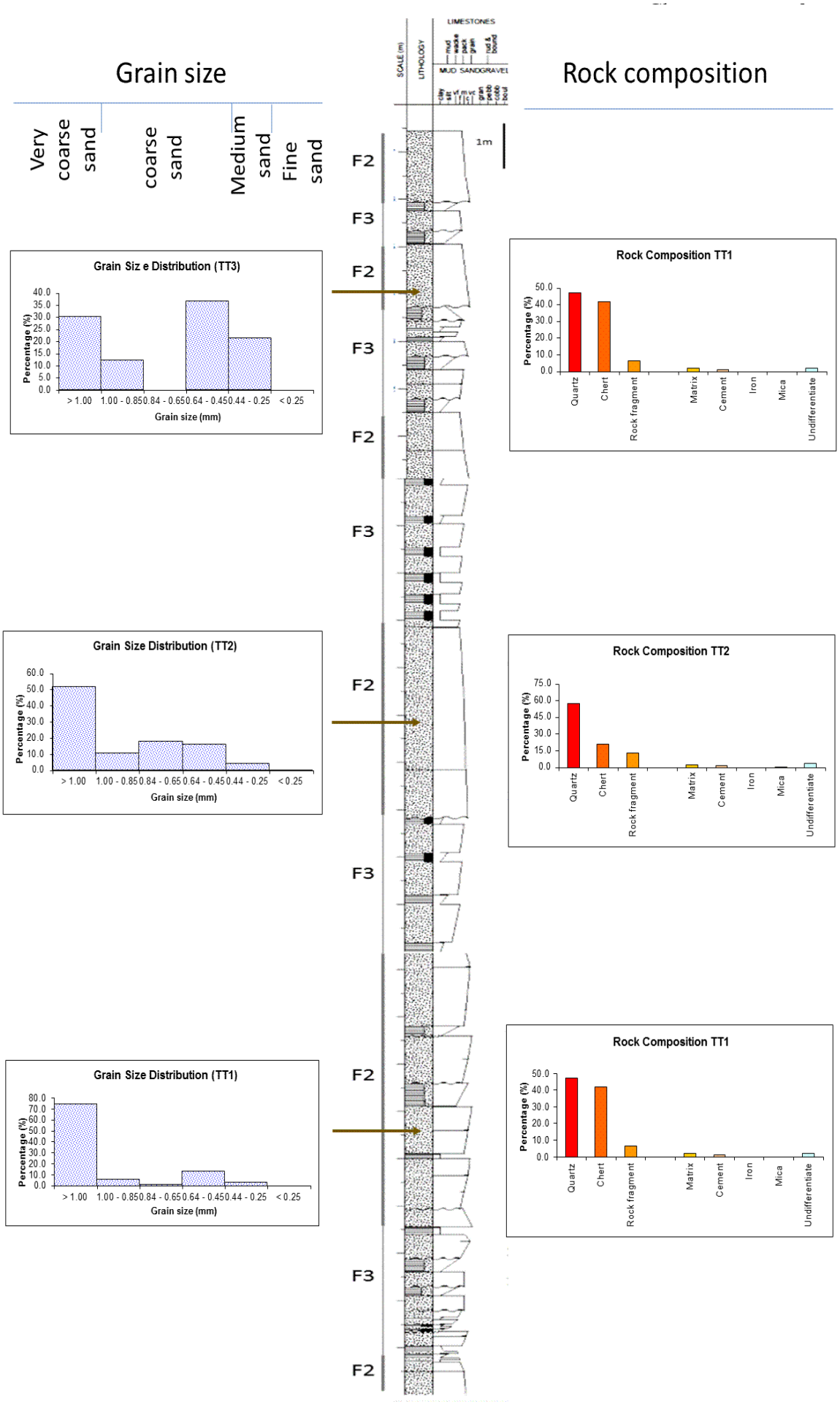

Fig. 5.14 Histogram of grain-size distribution and composition of Tatau Hill (locality L5) sandstone from thin sections.

Fig. 5.15 Hand specimen of quartz rich pebbly sandstone from TT2 at the lower section of Tatau Hill, locality L4.

Plate 5.10 Thin section of TT3 showing quartz overgrowth and pseudomatrix (in cycle) within the quartz grain at locality L4, Tatau Hill.

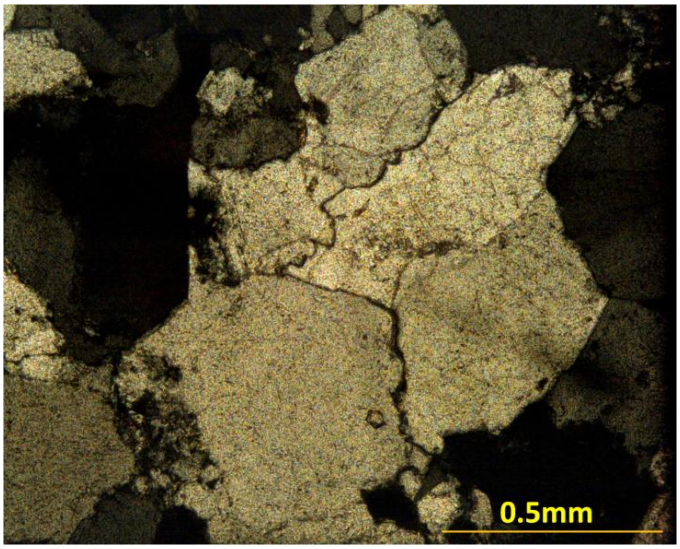

Plate 5.11 Thin section of TT1 showing concavo-convex contact of the quartz grains in locality L4, Tatau Hill.

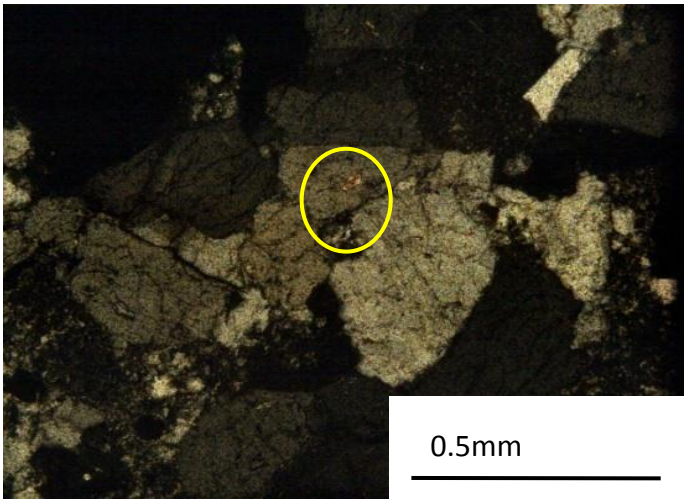

Plate 5.12 Thin section of TT1 showing mica inclusion with quartz grain similar to that in Plate 5.6 from Tutong Hill.

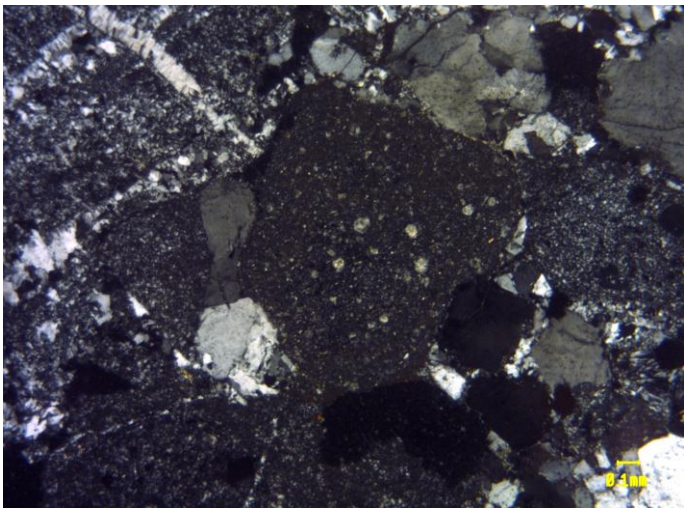

Plate 5.13 Thin section of TT2 showing radiolarian chert fragment with microcrystalline quartz at locality L4, Tatau Hill.

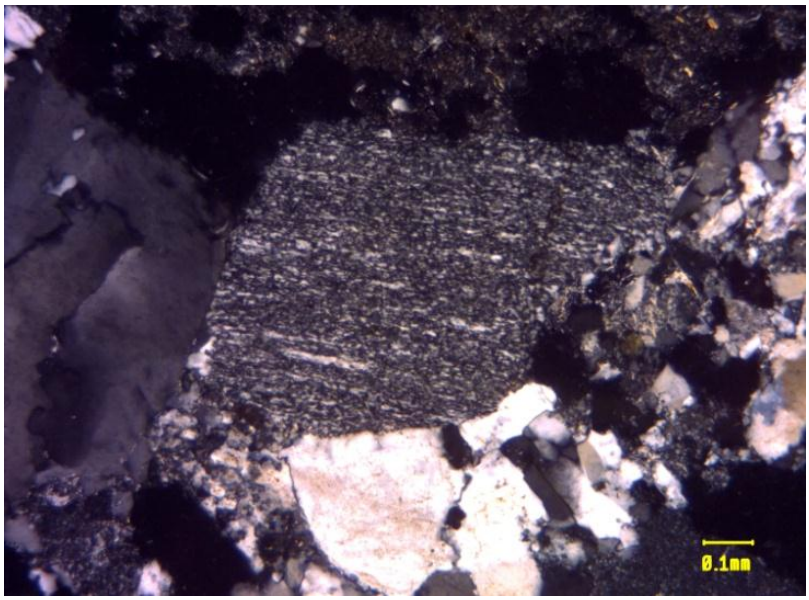

Plate 5.14 Thin section of TT3 showing angular schist fragment at locality L4, Tatau Hill.

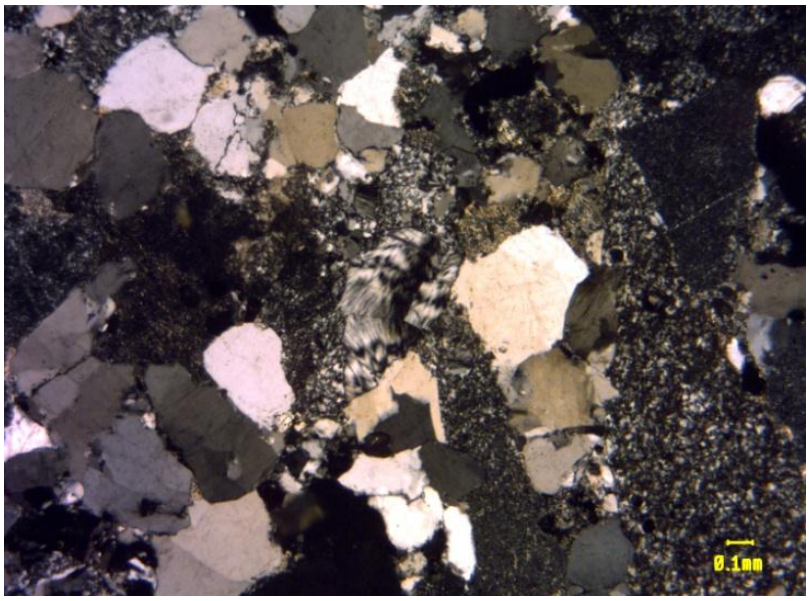

Plate 5.15 Spherulitic texture of the rhyolitic fragment that similar to rhyolite Piring Hill. Thin section of TT1 from locality L4, Tatau Hill.

Hormat Pasifik Quarry

The sandstone in the section is gradually changed from fine to medium grain sandstone to very coarse-coarse grain sandstone as the section becomes younger. The lower section is rich in grayish clay with a thin coal bed (Fig. 4.56) while the upper section is composed of quartz-rich pebbly sandstones. The composition of the sandstone is quartz (29% to 77%), rock fragments (10% to 33%) and less than 1% feldspars (Table 5.9). The QFL plot (Fig. 5.16) of the Hormat Pasifik Quarry samples shows that they are sublitharenites to litharenites.

Most of the sandstone samples are very poorly sorted and the grains are subangular to subrounded. The grains size ranges from fine to very coarse with fine to medium and very coarse being more common. Coarse grains are uncommon in the sandstone samples. The percentage of the matrix is between 2% and 6%, but more commonly 3%. Cement makes up 1% to 4% of the sandstone samples, but are most common from 2% to 3% (Table 5.11). The most common cement is silica which often forms overgrowths around the quartz grains (Plate 5.16).

The grain size distributions of the samples from the Hormat Pasifik Quarry exposures show a wide range (Table 5.11 & Fig. 5.18). Sample HL1 from the lowest part of the logged section, is negatively skewed with most of the grains in the range of fine to coarse sand , i.e. less than 0.25mm to 0.85mm. The standard deviation of the grain size distribution suggests very poor sorting (13.25). Sample HL2 shows fair distribution with the lowest grain size distribution of coarse sand from 0.65mm to 0.85mm (Fig. 5.18). The bed is very poorly sorted with standard deviation of 14.50

which is higher than in HL1. Sample HL3 shows a bimodal grain size distribution of coarse sand and very coarse sand (0.45mm-0.65mm and more than 1.00mm). The grain size distribution suggests a very poorly sorted bed with a standard deviation of 14.50. Sample HL4 has an average distribution from coarse sand to very coarse sand (0.22mm to more than 1.00mm) (Fig. 5.18) and is positively skewed. It is very poorly sorted as the standard deviation is 15.33. Sample HL5 is finer than HL1 to HL4 from fine to coarse sand, i.e. 0.25mm to 0.65mm (Fig. 5.18). It is negatively skewed and is mainly of medium sand. The sandstone is extremely poorly sorted with a standard deviation as high as 19.96. Sample HL6 shows bimodal grain size distribution with most of the grains being coarse to very coarse sand (0.45 – 0.85mm and more than 1.00mm) (Fig. 5.18). It suggests that the sediment was formed by a mixture of coarse and very coarse sand. The sandstone is poorly sorted with a standard deviation of 11.22. Sample HL7 is slightly negatively skewed with most of the grains in the range of medium to coarse sand (0.22 to 0.65mm) (Fig. 5.18). The bed is very poorly sorted with a standard deviation of 10.00 which is less than the older beds. Sample HL8 shows a bimodal grain size distribution of medium to very coarse sand (0.22-0.45mm and more than 1.00mm). There is insignificant coarse sand of grain size 0.65-0.85mm in the sample (Fig. 5.18). The distribution of grain sizes suggests a mixture of two dominant sand fractions of very coarse and medium sand. It is extremely poorly sorted with a standard deviation of 25.40. The youngest sample HL9 also shows bimodal distribution of coarse and very coarse sand (0.45-0.65mm and more than 1mm) (Fig. 5.18). The very coarse grains are mainly more resistant quartz; whereas less resistant grains such as chert are finer as just coarse grain. The graph is slightly negatively skewed with mainly medium to coarse sand. The sandstone is poorly sorted with a standard deviation of 10.59 (table 5.11).

The framework quartz grains are mostly polycrystalline quartz (14% to 39%) with strained (undulatory) extinction (Plate 5.16). Monocrystalline quartz is less common and makes up only 3% to 29% in the samples (Table 5.10). The quartz grains are generally subangular to subrounded and poorly sorted (Plate 5.17). Quartz overgrowth is commonly found and some of the quartz contains mica inclusions which is useful for provenance studies (Plate 5.18). Radiolarian chert is common making up to 23% presence in the sandstone (Plate 5.19). The chert grains are generally subrounded with spherical radiolarian skeletons replaced by micro quartz in them.

Rock fragments are found in all the sandstones. They include metamorphic rock fragments with micro quartz showing alignment in a schistose texture (Plate 5.19) (Adams et al., 1985). Igneous fragments similar to the Piring Hill rhyolite are also present in the sandstone (Plate 5.20). Some phyllosilicate fragments appear as clay pellets in the samples. Feldspar is rare (Plate 5.21) and almost completely altered in the samples making them difficult to identify.

Mineral	HL1		HL2		HL3		HL4		HL5	
		%		%		%		%		%
quartz total (quatz & chert)	88	84.6	241	67.3	397	83.2	402	78.5	427	88.0
Rock fragment	16	15.4	113	31.6	74	15.5	110	21.5	53	10.9
fedspars	0	0.0	4	1.1	6	1.3	0	0.0	5	1.0
TOTAL	104	100.0	358	100.0	477	100.0	512	100.0	485	100.0

Mineral	HL6		HL7		HL8		HL9	
		%		%		%		%
quartz total (quatz & chert)	430	78.2	419	80.9	215	57.2	406	85.7
Rock fragment	120	21.8	92	17.8	161	42.8	68	14.3
fedspars	0	0.0	7	1.4	0	0.0	0	0.0
TOTAL	550	100.0	518	100.0	376	100.0	474	100.0

Table 5.9 Mineral composition of the pebbly sandstone and sandstone samples from the Hormat Pasifik Quarry. HL1 to HL9 are from bottom to top of thin section.

Quartz type (%)	HL1	HL2	HL3	HL4	HL5	HL6	HL7	HL8	HL9
Polycrystalline,<3	3.8	9.5	7.7	4.3	4.8	3.4	7.1	3.8	6.5
polycrystalline, >3	23.1	9.5	30.8	13	9.5	24.1	21.4	30.8	32.3
undulatory quartz	61.5	52.4	53.8	69.6	61.9	65.5	57.1	57.7	58.1
monocrystalline	11.5	28.6	7.7	13	23.8	13.8	14.3	7.7	3.2

Table 5.10 Framework quartz grains of the samples from thin-section point-counts.

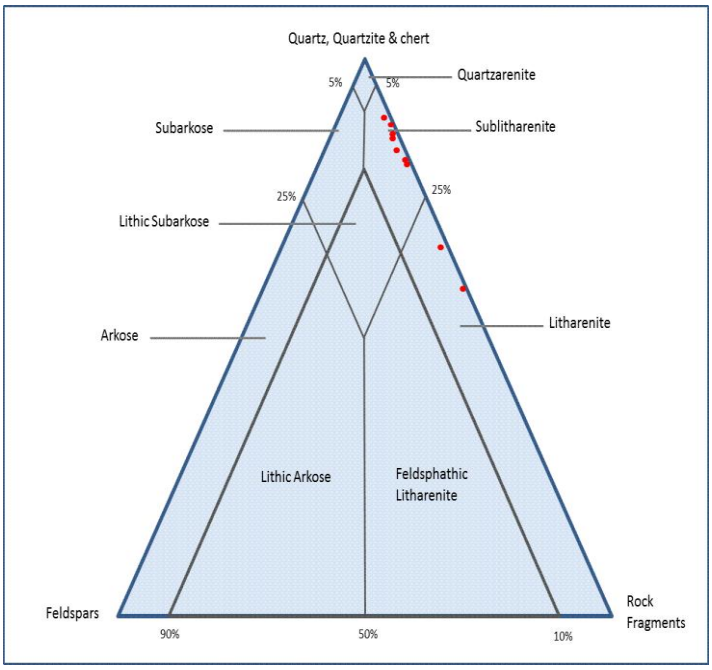

Fig. 5.16 Hormat Pasifik Quarry sandstone samples plotted in Mc. Bride's (1953) classification chart.

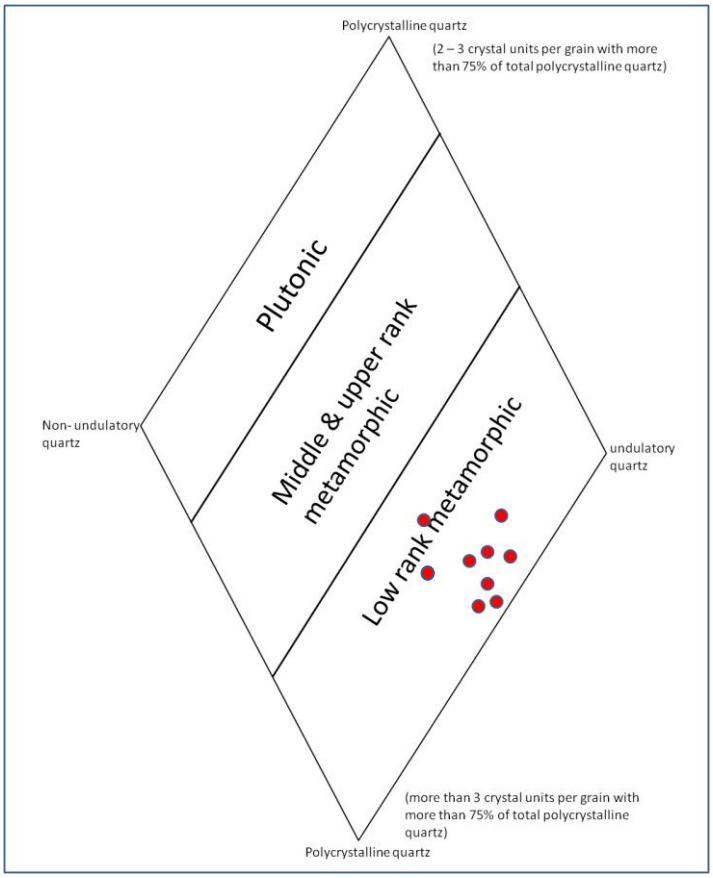

Fig. 5.17 Quartz grain provenance in Basu et al. (1975) classification chart of specimens from Hormat Pasifik Quarry.

Grain Size (mm)	HL1		HL2		HL3		HL4		HL5	
		%		%		%		%		%
> 1.00	-		87	24.10	166	35.85	141	31.19	-	
1.00 - 0.85	-		60	16.62	32	6.91	62	13.72	-	
0.84 - 0.65	16	14.95	16	4.43	40	8.64	66	14.60	26	5.15
0.64 - 0.45	26	24.30	37	10.25	167	36.07	91	20.13	216	42.77
0.44 - 0.25	18	16.82	87	24.10	53	11.45	88	19.47	210	41.58
< 0.25	47	43.93	74	20.50	5	1.08	4	0.88	53	10.50
TOTAL	107	39.25	361	100.00	463	100.00	452	100.00	505	100.00
Varians		175.49		63.21		234.87		98.59		398.45
Std Dev. (Sorting)	(V. Poor)	13.25	(v. Poor)	14.50	(V. Poor)	15.33	(V. Poor)	9.93	(Ex. Poor)	19.96

Grain Size (mm)	HL6		HL7		HL8		HL9	
		%		%		%		%
> 1.00	126	23.03	-		134	40.12	90	20.09
1.00 - 0.85	34	6.22	80	15.47	23	6.89	15	3.35
0.84 - 0.65	187	34.19	92	17.79	-		89	19.87
0.64 - 0.45	114	20.84	158	30.56	47	14.07	145	32.37
0.44 - 0.25	43	7.86	152	29.40	90	26.95	109	24.33
< 0.25	43	7.86	35	6.77	40	11.98	-	
TOTAL	547	100.00	517	100.00	334	100.00	448	100.00
Varians		125.84		100.07		181.14		112.24
Std Dev. (Sorting)	(V. Poor)	11.22	(V. Poor)	10.00	(Ex. Poor)	25.40	(V. Poor)	10.59

Table 5.11 Grain size distribution of the pebbly sandstone and sandstone samples from Hormat Pasifik Quarry.

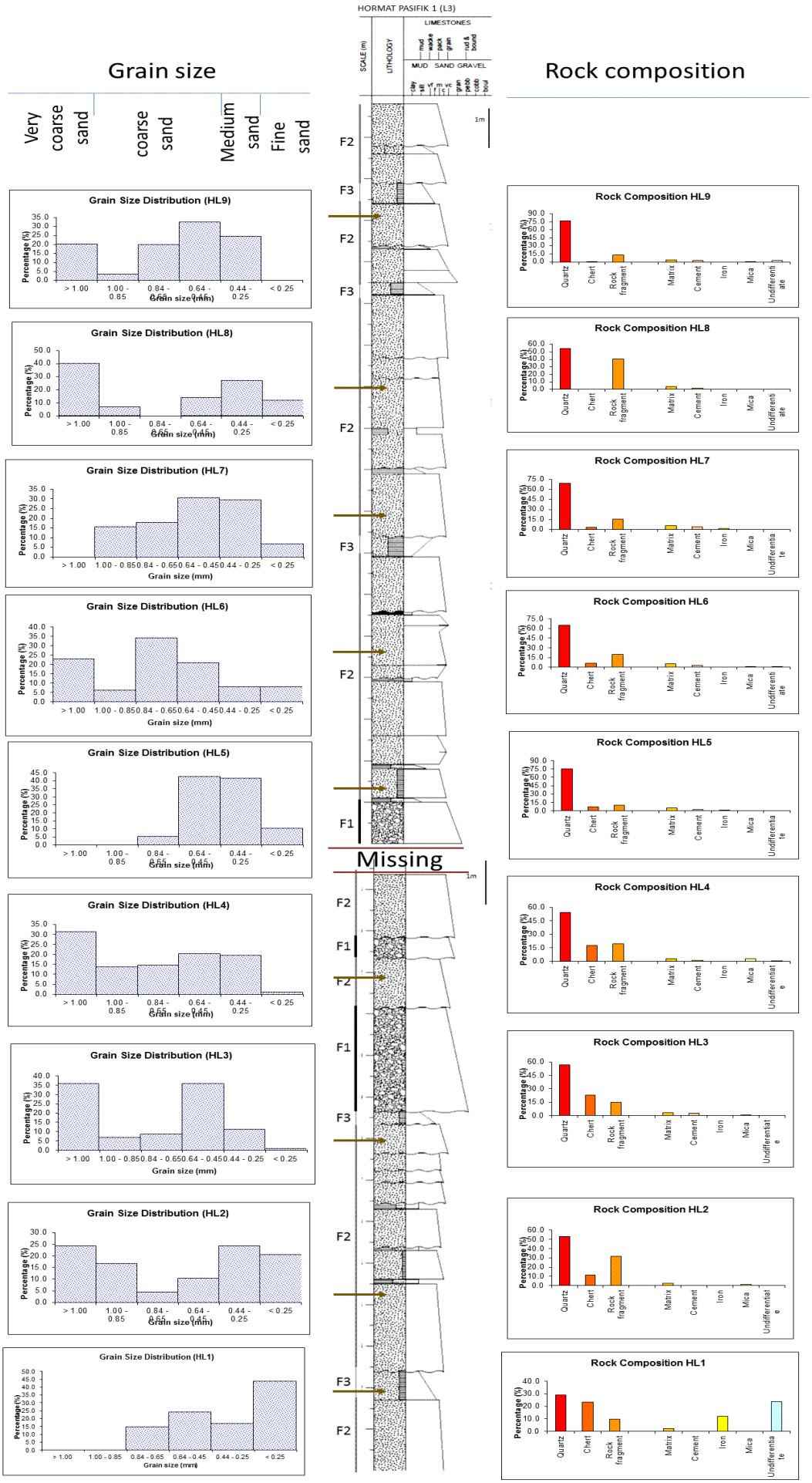

Fig. 5.18 Histogram of grain-size distribution and rock compositions of Hormat Pasifik Quarry (locality L3 & L8) sandstone from thin sections.

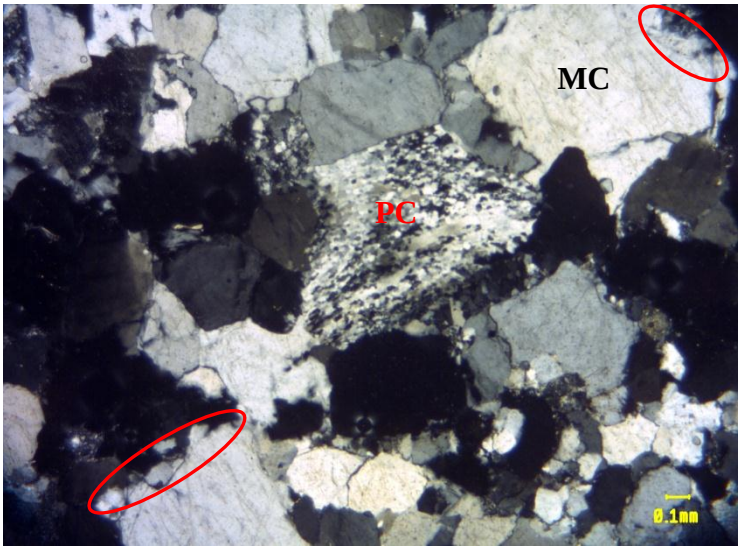

Plate 5.16 Thin section of sample HL2 showing monocrystalline (MC), polycrystalline (PC) quartz grains and overgrowth of silica cement around quartz grains (red circle).

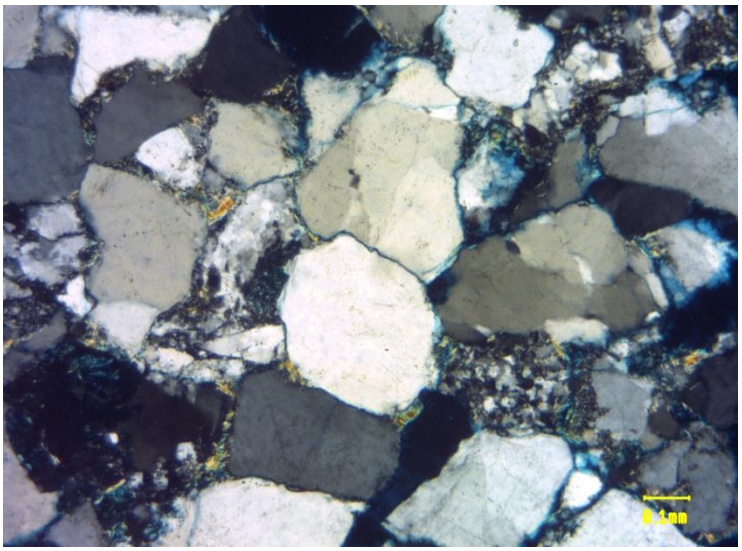

Plate 5.17 Thin section of sample HL5 showing sub-angular to sub-rounded quartz grains with concavo-convex contact and pseudomatrix in the sample.

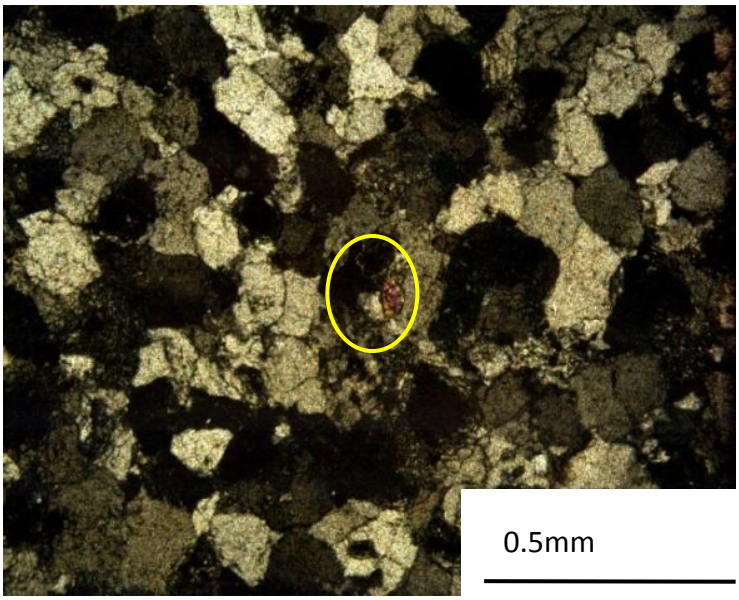

Plate 5.18 Thin section of sample HL7 showing mica inclusion (in circle) within quartz grains for source provenance.

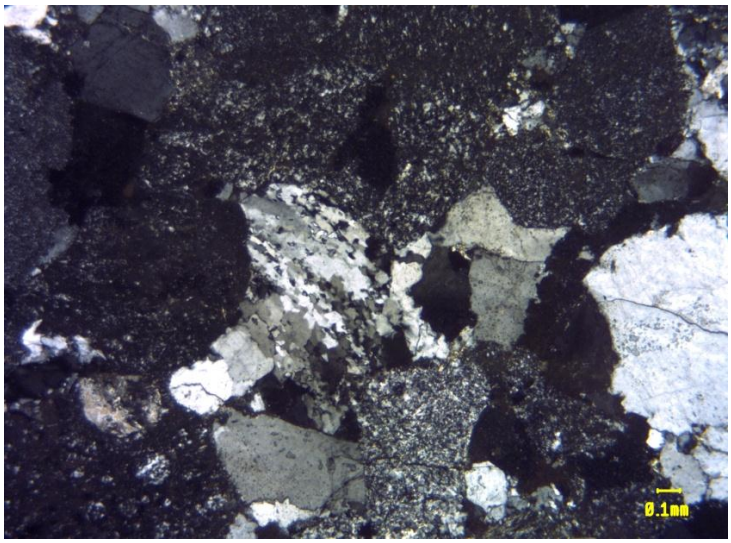

Plate 5.19 Thin section of sample HL5 showing radiolarian chert with microcrystalline quartz and polycrystalline quartz.

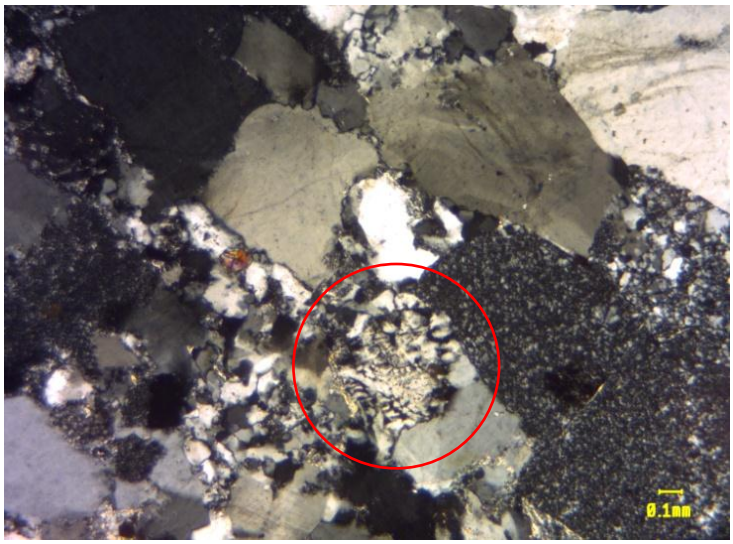

Plate 5.20 Thin section of sample HL2 showing spherulitic texture of rhyolitic igneous rock fragment (Circle) that similar to the rhyolite rock in Piring Hill, Tatau.

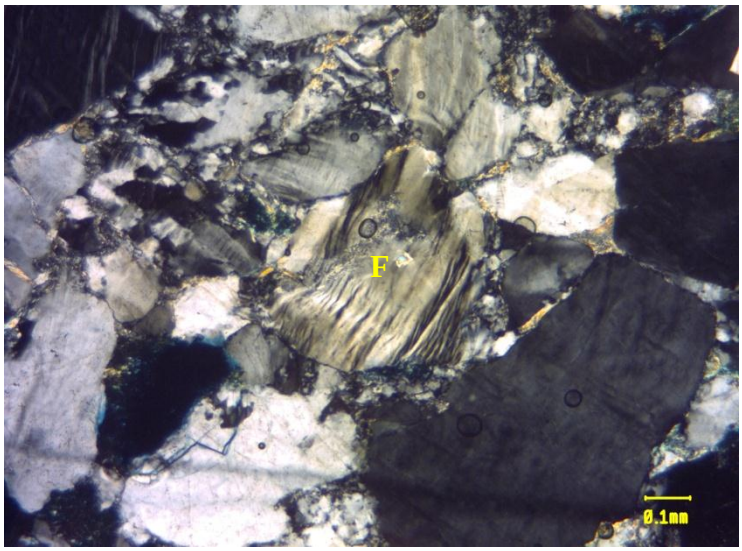

Plate 5.21 Thin section of sample HL8 showing angular feldspar (F) with strained albite twinning.

5.3 PETROGRAPHY OF THE PELUNGAU HILL

The clasts in the conglomerate beds at the Pelungau Hill outcrop are composed of shale, sandstone and some metasediment fragments. The conglomerate beds are grain-supported at the base and turns gradually to matrix-supported towards its upper section (Fig. 5.19). The subrounded to well rounded clasts are very poorly sorted and from 5cm to over 35cm in size (Fig. 5.20). The dominant soft sandstone and shale clasts tend to be very well rounded (Table 5.12). The percentage of the matrix is about 20% and up to 40% towards upper part of the beds.

The shale and sandstone fragments tend to be well rounded compared to those from Ransi Hill, Tutong Hill and Tatau Hill conglomerate clasts (Fig. 5.20). These clasts are softer and less durable and would not have survived more than one cycle of deposition as they would generally break down into finer sizes otherwise (Pettijohn, 1975).

The matrix of the Pelungau Hill conglomerate is mainly of silt and clay. Some parts of the matrix are cemented and stained by iron oxide. The conglomerates beds consist of the well-rounded clasts ranging from 2cm to as big as 25cm across (Fig. 5.20). The clast sizes vary from bed to bed but in general decrease upsection. Most of in the beds are generally normally graded. The well rounded clasts suggest their being transported some distance from the source and deposited in a fluvial environment (Seiders & Blome, 1988). This is consistent with the sedimentary structures and palaeocurrents study in the area.

Based on the composition of the conglomerates, the clasts are relatively unstable as they are composed of about 90% shale and sandstone. The conglomerate is classified as a polymict conglomerate based on its mixed lithology that shown in Fig.5.20.

Fig.5. 19 A few faults (red dotted line) that cuts into the conglomerate beds (C).

Fig.5. 20 Conglomerate bed that composed of rounded sandstone (Sst) and shale (Sh) clasts in Pelungau outcrops (locality L6).

5.4 DIAGENESIS

The term diagenesis has been applied in various ways to the post-depositional, pre-metamorphic processes which affect a sediment (Selley, 1988). Diagenesis refers primarily to the reactions which take place within a sediment between one mineral and another or between one or several minerals and the interstitial fluids (Pettijohn, 1957). The effects of diagenetic processes on rock properties such as porosity and the degree of lithification are progressive. Diagenesis includes many chemical and physical processes that are also active during deposition, weathering and metamorphism (Fred, 2005). There are four major processes involved in diagenesis namely compaction, solution, cementation and neomorphism. This complicates diagenesis basically because their unstable mineralogy and high initial permeability make them susceptible to percolating reactive fluids (Selley, 1992).

Microstylolites provide evidence of solution on a much larger scale than commonly seen in limestones (Carozzi & Von Bergen, 1987). Stylolites are usually parallel or sub-parallel to bedding. The microstylolites which occurred between two grains can be formed at burial depths as shallow as 90m (Shlanger, 1964). This stylolitization process provides evidence for extensive solution of carbonate during deep burial (Selley, 1992) and might have contributed to the large amount of carbonate cement seen in the Arip limestone succession.

Physical deformation due to the compactional stresses lead to the loss of porosity which can be seen under thin section. Pseudomatrix is formed as rock fragments alter to clays under pressures (Plate 5.22; 5.23). The increase in the amount of pseudomatrix which resulted from the mechanical compaction of mud intraclasts

during burial suggests incorporation of these mud intraclasts into the sandstones during relative sea-level changes (Shanley and McCabe, 1994). Another common compactional fabric is pressure solution where grain boundaries undergo dissolution and recrystallization. The concavo-convex contact between quartz grains were formed by the dissolution at the points of maximum compactional stress as the sediment was compacted. Long contacts between the grains was commonly found in thin sections of the Ransi Member samples indicating high compaction of the rock (Plate 5.24). Pressure solution is better developed in finer sandstone than in coarser sandstone due to the coarser grains having bigger surface areas (Kim & Lee, 2004).

Dissolution of the minerals is insignificant in the Ransi Member samples but the Arip Limestone shows significant dissolution feature such as stylolites (Plate 5.25). Quartz overgrowth or cementation is the most common type of cement in the pore spaces in these samples of Ransi Hill, Hormat Pasifik Quarry, Tatau Hill and Tutong Hill (Plate 5.26) probably due to the response in groundwater flow with increasing ionic concentration in pore waters and increased burial temperatures. The overgrowths or microcrystalline quartz cement occurred when high pore-water concentrations of hydrous silica were present. Calcite cement is common for the Arip and Lesong outcrop samples (Plate 5.27) while quartz overgrowth is common in the Ransi Member rocks (Fig. 5.24).

The radiolarians in the chert of originally siliceous hard parts in rounded form were replaced by microcrystalline quartz (Plate 5.28; 5.29; 5.30). Recrystallization occurred where the existing mineral retains its original chemistry but increases in size

and changes its volume. This was observed in thin section of the rounded microcrystalline quartz from hard part of radiolarian.

The multiple diagenetic episodes and burial history have affected the porosity and permeability of the rocks that it might decrease the pore space with late quartz cementation and pressure dissolution that form concavo-convex contact between grains. The sandstone of the Ransi Member had been commonly subjected to intergranular pressure solution and quartz cementation producing concavo-convex contacts in Arip Member sandstone and stylolitic contacts in Arip limestone. The depth of burial was probably more than 1000m before the rocks were being uplifted and exposed (Boggs, 1992).

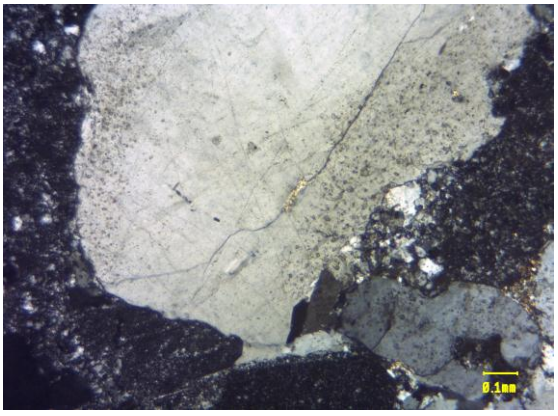

Plate 5.22 Pseudomatrix at the edge of the big quartz grain.

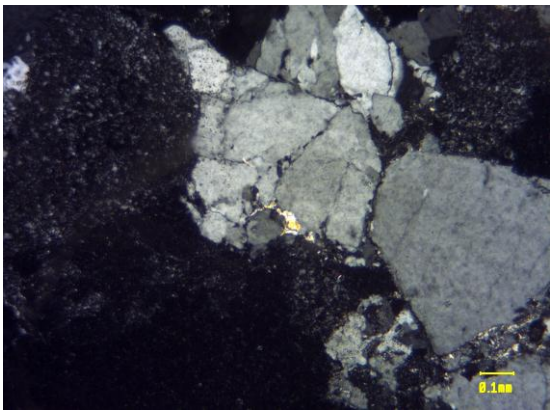

Plate 5.23 Clay pseudomatrix around the quartz grains.

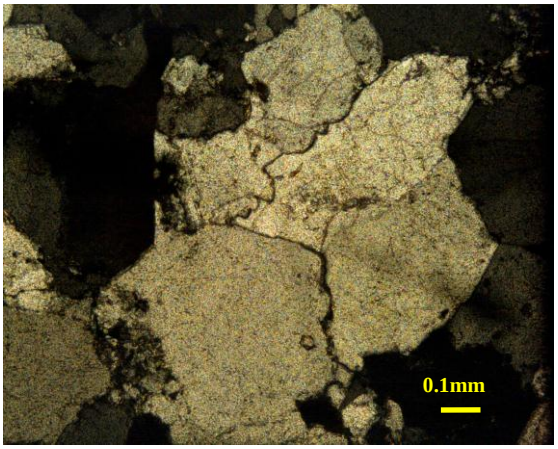

Plate 5.24 Pressure solution between quartz grains. Thin section of sample from locality L2,Tutong Hill.

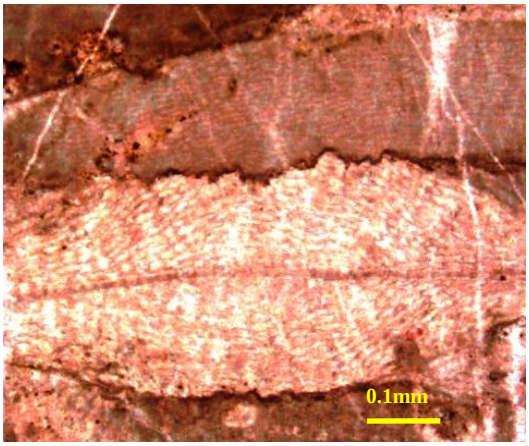

Plate 5.25 Stylolitic structure in the Arip limestone. Thin section of sample from locality L10.

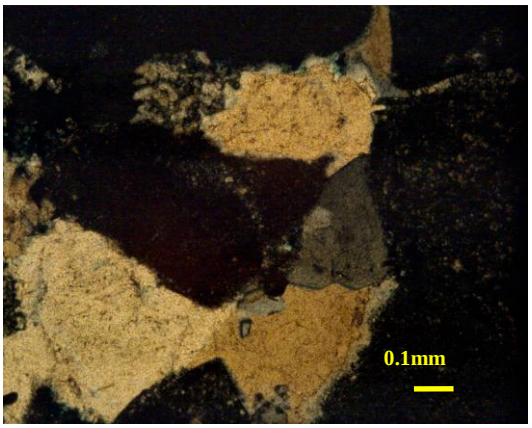

Plate 5.26 Overgrowth of quartz around quartz grain. Thin section of sample from locality L3, Hormat Pasifik Quarry.

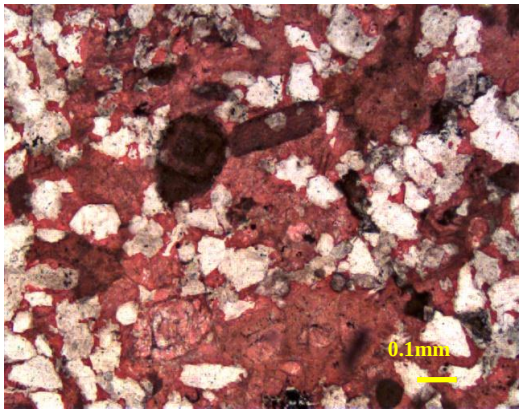

Plate 5.27 calcite cementation around the quartz grain in the Lesong. Thin section of sample from locality L9.

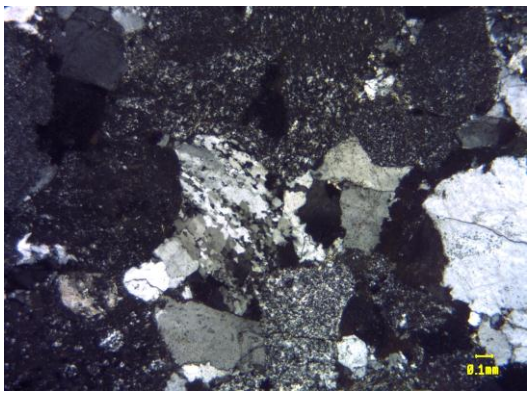

Plate 5.28 Microcrystalline quartz replacing radiolarian in chert. Thin section of sample from locality L5, Tatau Hill.

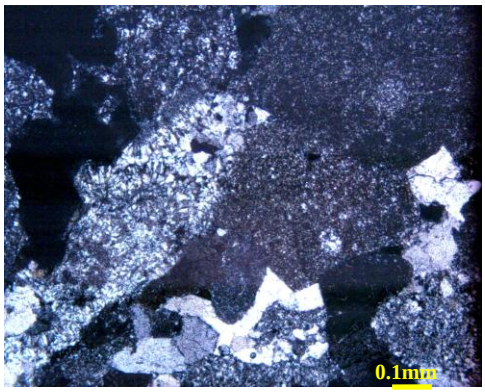

Plate 5.29 Rounded microcrystalline quartz in the chert fragments. Thin section of sample from locality L2, Tutong Hill.

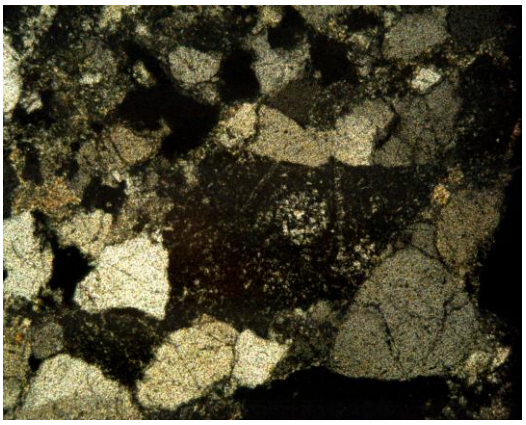

Plate 5.30 Microcrystalline quartz growth replacing radiolaria the chert. Thin section of sample from L8, Hormat Pasifik Quarry.

5.5 PETROGRAPHY OF THE LESONG HILL CALCAREOUS SANDSTONE

The Lesong Hill outcrop is an isolated outcrop of calcareous sandstone (2.5m X 2m) located at the edge of Tatau Formation near the major Anak-Nyalau Fault (See Fig. 4.1). It could be just a large block dislocated by the fault. The absence of diagnostic fossils makes correlating it with other outcrops difficult.

The fine grained calcareous sandstone is composed of monocrystalline quartz (Plate 5.31) cemented by calcite (stained red using potassium ferricyanide in Plate 5.31 and Plate 5.32). Some gastropod and foraminifera fragments were observed in the thin sections but none are diagnostic in terms of age but useful for palaeoenvironment interpretation.

The calcite present is mainly fine to medium sparry calcite forming pore filling cement (Plate 5.31).

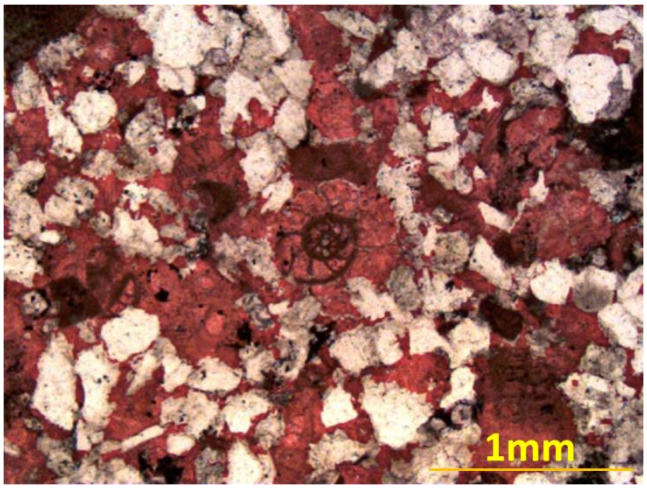

Plate 5.31 Under plan-polarized thin section of calcareous sandstone with a foraminifera fragments. Calcite stainned red with potassium ferricinite.

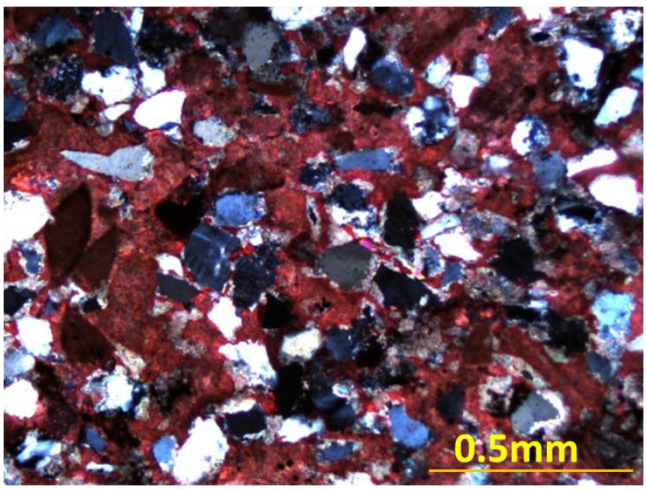

Palte 5.32 Thin section under x-nicol of Lesong Hill calcareous sandstone with sub- angular to sub-rounded monocrystalline quartz.

5.6 PETROGRAPHY OF THE PIRING HILL RHYOLITE

A rhyolitic porphyry dyke has intruded into the Eocene metasediments at Piring Hill located 7km to the southwest of the Tatau area (Fig. 4.2). Five thin sections were made from 5 samples and 2 samples were sent to Washington State University for geochemical analysis by XRF.

The general composition of the porphyry is shown in Table5.12. The size of phenocrysts in the porphyry is from 1-2mm. The porphyritic texture is shown in Plate 5.33. Spherulitic and myrmekite textures are common in the Piring Hill porphyry (Azman A. Ghani,1997; Shelley, 1992; Swanson et al., 1989). The rhyolite is porphyritic with phenocrysts of plagioclase, K-feldspar and quartz (Plate 5.34). The phonocrysts are generally euhedral. Vesicles are common in the rock.

The groundmass of quartz and feldspar forms between 22% to 37% of the rock (Table 5.13) around the phenocrysts. Some of the groundmass are present as sheaf-like growths of quartz-feldspar crystals radiating from the euhedral phonocrysts (Plate 5.35). The mineral composition of the groundmass is same as the phenocrysts.

The quartz phenocrysts are angular and coarse grained (about 0.3mm to 1mm across) with sharp crystal boundaries (Plate 5.35). The grains are clear with non-undulatory uniform extinction. They are commonly present as nucleic for the spherulitic growth around it. The groundmass quartz grains as observed in thin section is generally less than 0.1mm across. The multiple albite-twinned plagioclase is present as both phenocrysts and groundmass. The K-feldspar is Carlsbad twinned (Plate 5.34). The

cloudiness of the feldspar observed under PPL is due to the patchy alteration of the minerals to fine-grained sericite. Muscovite is present in some of the samples and some of it was formed as a result of hydrothermal alteration in the pore spaces or along fractures. They are elongated crystals with high birefringence (Plate 5.34). Greenish chlorite is also found together with the muscovite in the fractures and vacuoles as detrital flakes as an alteration product of volcanic fragments or an authegenic mineral filling the pores.

The spherulitic texture suggests that the magma had undergone a high degree of undercooling and thus the crystal habit is partly suppressed so that the groundmass tends to crystallize rapidly outwards in all directions with the phenocrysts as nuclei (Azman, 1997) (Plate 5.35). Spherulites are formed under conditions of high-viscosity fluids (Keith and Padden, 1963). This texture indicates diffusion to be dominant rate-limiting function during crystallization (Selley, 1992).

The porphyritic texture shown by the rhyolite indicates that the magma first cooled at depth to form the phenocrysts of plagioclase, k-feldspar and quartz (Azman, 1997). The remaining melt of about 50% of the magma subfrequently experienced a sudden and rapid cooling that formed the groundmass and spherulitic texture due to the rapid intrusion (Leake, 1990) triggered by the Anak-Nyalau faulting to the southeast of the Tatau area. This sudden emplacement process resulted in rapid quenching of the remaining liquid with crystallization outwards in all directions from the pre-existing phenocrysts as focus of nucleation (Swanson, et al,. 1989).

Two representative samples selected from two localities in Piring Hill were sent to Washington State University and analyzed for major and trace elements. The result of the geochemical analysis is given in Table 5.14. The Piring volcanic is silica saturated (76%) according to its plot in the TAS (total alkalis-silica) diagram that recommended by I.U.G.S (Le Mitre et. al., 1989) for the classification of volcanic rocks. Both the samples fall in rhyolite field (Fig. 5.21). In general the Piring Hill rhyolite is characterized by rather high contents of SiO2 (76%), Al_2O_3 (12.3%-12.4%), K_2O+Na2O (8.06%-8.25%), FeO (1.93% - 1.97%), Rb (196.3ppm-205.6ppm), Ce (76.99ppm -77.92ppm) and Y (50.15ppm – 50.77ppm) and relatively low TiO_2 (0.20%), MnO (0.029%), MgO (0.11% - 0.27%) and P_2O_5 (0.023% - 0.024%) (Table 5.14).

According to the K_2O vs. SiO_2 diagram, the samples are placed in the high K-calc alkaline field (Fig. 5.22). It suggests dry water-undersaturated conditions during crystallization of the rhyolite. The felsic volcanic rhyolite is characterized by high total REE contents and has a pronounced negative Eu anomaly (Table 5.13; Fig. 5.23). Whereas, REE relative to the normal mid-ocean ridge basalts (MORB), the studied rhyolite show strong depletion in Ta, Nb, Eu and Ti (Fig. 5.24). Such anomalies may be attributed to fractionation of plagioclase (Eu depletion) and ilmenite (Ti depletion).

Tectonic discrimination diagrams (Fig. 5.25) of Rb vs. Nb + Y and Nb vs. Y indicate an alkaline-type post collision granite (Pearce, 1996). The felsic volcanic rock is distributed in between the fields of volcanic arc and within plate granites suggesting that then Piring rhyolite dyke was form as a result of extension in the post-collisional period during which the oceanic crust might have broken off from the continental crust (Fig. 5.26).

Minerals (%)	Thin sect. 1	Thin sect. 2	Thin sect. 3	Thin sect. 4	Thin sect. 5

Total of Minerals Present

Quartz (phenocrysts)	23 %	22.3 %	15 %	35 %	19.3 %
Plagioclase (Phenocrysts)	26.6 %	25 %	39.5 %	27 %	37.5 %
K-feldspar (Phenocrysts)	15.4 %	15.5 %	18 %	11.7 %	21.2 %
Groundmass	35 %	37.2 %	27.5 %	26.3 %	22 %

Table 5.12 Average percentage of the Piring Hill igneous body.

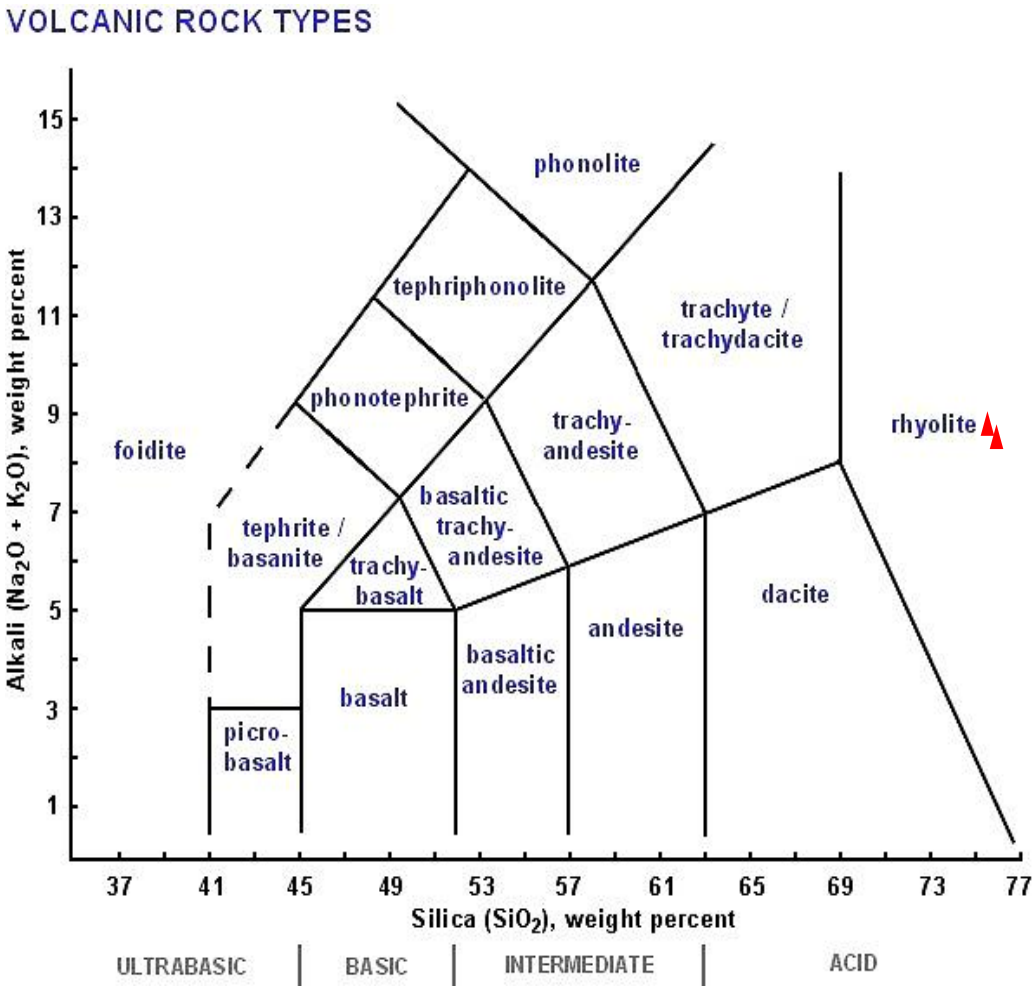

Fig. 5. 21 Total alkalis-silica (TAS) diagram for the studied of the Piring Hill volcanic rock (after Le Maitre et. al., 1989).

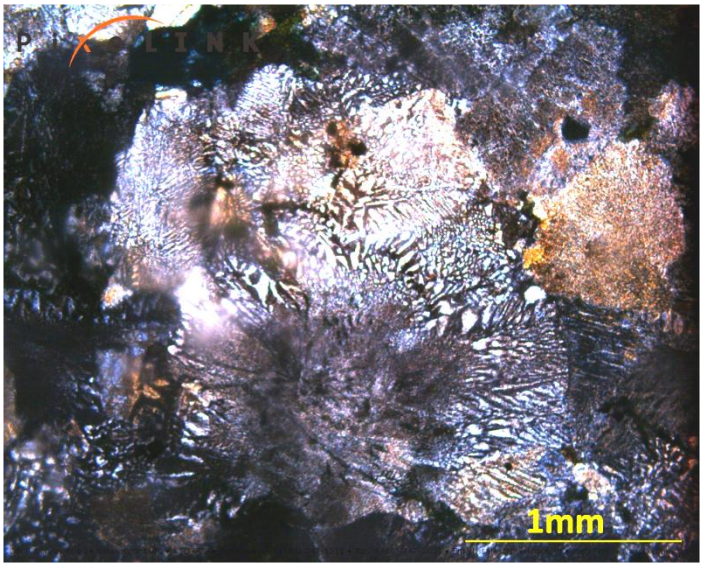

Plate 5.33 Thin section of rhyolite from Piring Hill showing spherulitic texture (flower like form).

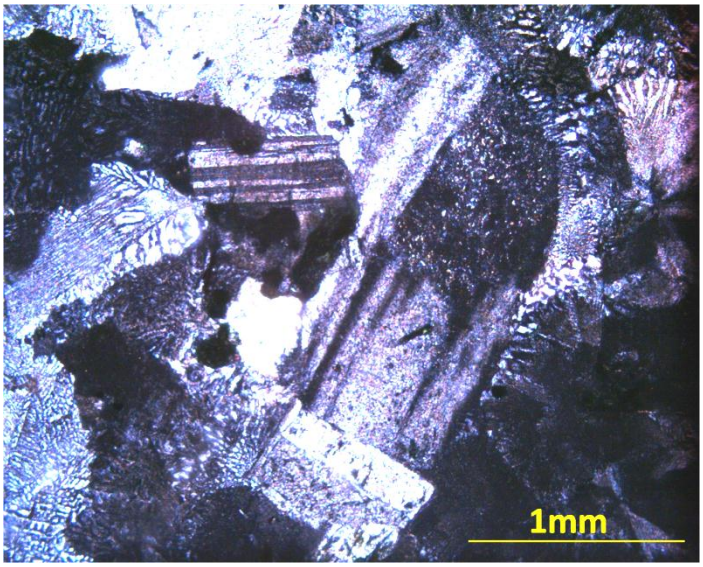

Plate 5.34 Thin section of Piring Hill intrusion showing plagioclase phenocrysts with sperulitic growth texture.

Plate 5.35 Thin section of Piring Hill rhyolite under PPL showing sheaf-like growth in quartz phenocrysts.

Plate 5.36 Muscovite (red circle) in pore space of Piring Hill rhyolite thin section.

Sample (%)	L008	L009
SiO_2	75.96	76.06
TiO_2	0.203	0.200
Al_2O_3	12.33	12.36
FeO*	1.93	1.97
MnO	0.029	0.029
MgO	0.27	0.11
CaO	1.20	1.00
Na_2O	3.29	3.52
K_2O	4.77	4.73
P_2O_5	0.024	0.023
Total	100.00	100.00

Ni	6	7
Cr	172	169
Sc	7	7
V	7	6
Ba	504	482
Rb	199	210
Sr	41	49
Zr	305	303
Y	54	54
Nb	13.3	13.0
Ga	18	16
Cu	12	9
Zn	59	56
Pb	25	24
La	39	40
Ce	76	76
Th	19	19
Nd	36	34
U	5	5
Cs	5	8

NiO	7.9	9.0
Cr_2O_3	251.5	247.3
Sc_2O_3	11.4	11.2
V_2O_3	9.6	9.3
BaO	563.2	538.3
Rb_2O	217.2	230.0
SrO	48.6	57.6
ZrO_2	411.9	409.3
Y_2O_3	67.9	67.9
Nb_2O_5	19.0	18.6
Ga_2O_3	24.2	22.0
CuO	14.6	11.4
ZnO	73.9	69.9
PbO	26.5	26.1
La_2O_3	45.7	46.9
CeO_2	93.7	93.4
ThO_2	21.0	20.6
Nd_2O_3	41.5	39.4
U_2O_3	5.6	5.3
Cs_2O	5.6	8.7

Sample (ppm)	L008	L009	Chondrite	P-Mantle	EMORB
La	38.09	37.60	0.235	0.69	6.30
Ce	77.92	76.99	0.676	1.78	15.00
Pr	9.22	9.07	0.089	0.28	2.05
Nd	35.19	34.50	0.452	1.35	9.00
Sm	8.31	8.05	0.147	0.44	2.60
Eu	0.66	0.68	0.056	0.17	0.91
Gd	8.25	8.12	0.196	0.60	2.97
Tb	1.50	1.47	0.036	0.11	
Dy	9.29	9.17	0.243	0.74	3.55
Ho	1.92	1.90	0.056		0.79
Er	5.34	5.17	0.159	0.48	2.31
Tm	0.78	0.77	0.024	0.07	
Yb	4.79	4.78	0.163	0.49	2.37
Lu	0.73	0.73	0.024	0.07	0.35
Ba	507	487			
Th	18.76	18.77			
Nb	12.74	12.51			
Y	50.77	50.15			
Hf	7.89	7.96			
Ta	1.22	1.17			
U	3.82	3.92			
Pb	23.46	22.86			
Rb	196.3	205.6			
Cs	4.46	4.76			
Sr	40	47			
Sc	7.1	6.9			
Zr	287	291			

Table 5.13 Major and trace element composition for calculated normative minerals of the Piring Hill rhyolite from XRD analyses.

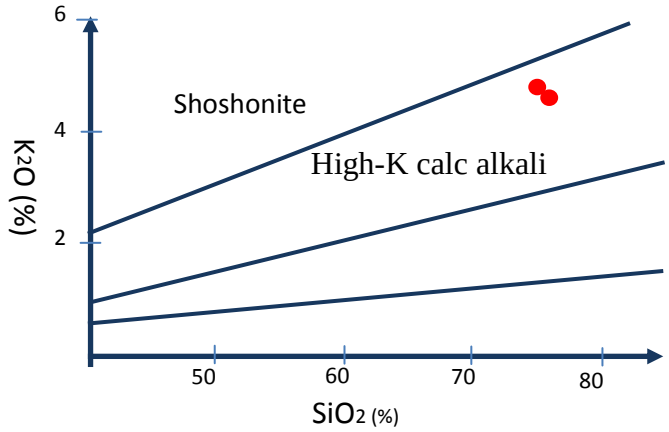

Fig. 5.22 Major element plot of K_2O vs. SiO_2 for the Piring rhyolite. It shows a high-K calc alkali affinity.

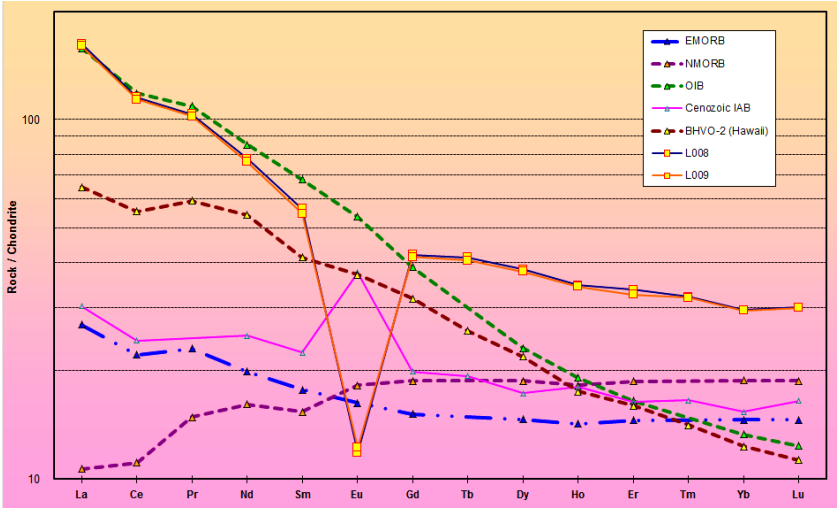

Fig. 5.23 Chondrite-normalized REE profiles (normalizing values after McDonough & Sun, 1995) for the rhyolite. The Eu was low for both of the Piring Rhyolite dyke samples (L008 & L009).

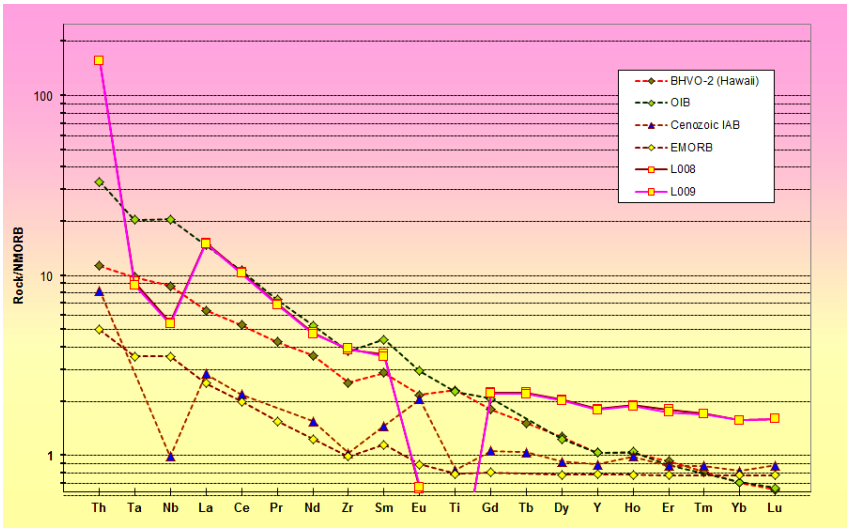

Fig. 5. 24 Mid-ocean ridge basalts (MORB)-normalized REE profiles(normalizing values after McDonough & Sun,1995) for the rhyolite showing strong depletion of Ta, Nb, Eu and Ti that might attributed to fractionation of plagioclase and ilmenite (sample L008 & L009).

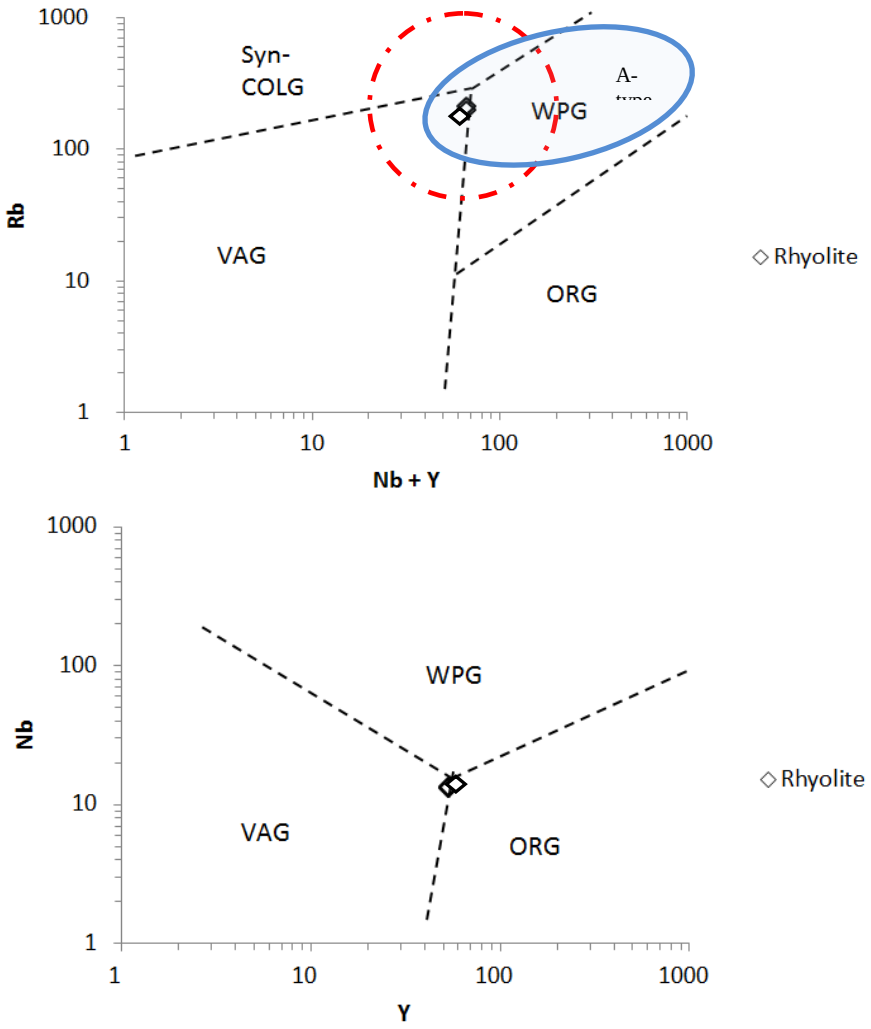

Fig. 5.25 Tectonic discrimination diagrams illustrating tectonic setting of the Piring Hill rhyolite: (a) Rb vs. Nb+Y diagram (Pearce et al., 1984), The A-type granites field in (a) is after Whalen et al. (1987) and red cycle of post-collision granites is after Pearce (1996); (b) Nb vs. Y diagram (after Pearce et al., 1984).

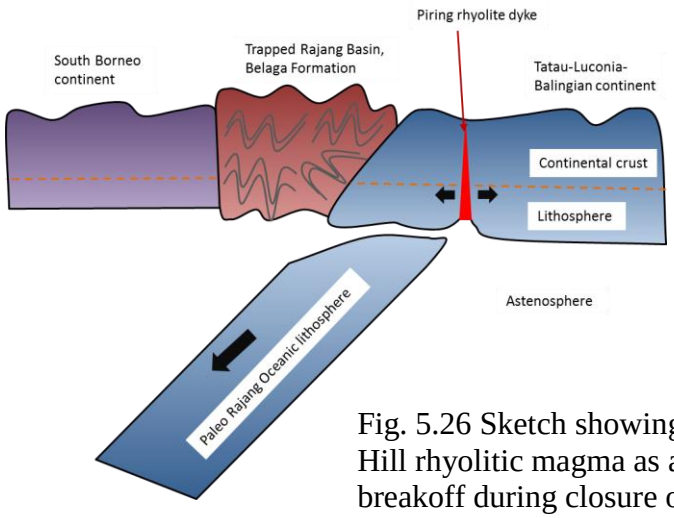

Fig. 5.26 Sketch showing the generation of Piring Hill rhyolitic magma as a consequence after slab breakoff during closure of Ranjang Sea (modified after Moghazi, 2003).

5.7 PETROGRAPHY OF THE ARIP LIMESTONE

Limestones are rocks whose primary constituents are composed of calcium carbonate (Nockolds et al., 1978). Carbonate rocks comprise material formed mostly at or near the site of final accumulation of the sediment. Much of the material is produced by biological processes (Adams et al., 1985). Two most carbonate minerals common in limestone are calcite and dolomite (Boggs, 1992). Therefore, potassium ferricyanide in weak acid solution is used to help in distinguishing dolomite from calcite. The calcite would be stained red while the dolomite remains white.

The foraminifera rich limestone in the project area are found at the two locations, namely the Arip Nursery and Arip Cave areas (Fig.4.2).

Arip Cave Limestone

The Arip Cave Limestone is composed of sparry calcite, bioclast (microfossils) and some micrite. It is rich in larger benthonic foraminifera making up to 80% of the rock while micrite makes up between 10% to 20% of the rock. The original components of the limestone were not organically bound together during deposition and it was grain supported. This is very little micrite and the rock is classified as a packstone (Dunham, 1962) from cut-sections of hand specimens.

Under thin section, the Arip Cave limestone was observed to be grain-supported with sparry calcite cement. The grains in the limestone are loosely-packed, suggesting early cementation before significant compaction. The allochems are a mixture of

peloids and bioclasts with the ratio of bioclasts to peloids being 3:1. It is therefore a poorly sorted biosparite according to Folk's (1962) classification (Plate 5.37).

The bioclasts are mainly foraminifera and coralline red algae. Some foraminifera fragments are filled with micrite in their chambers. The foraminifera are miliolids with micritic walls (Plate 5.38).

Details on the fossils will be further discussed under the Palaeontology section (chapter 4.3.3).

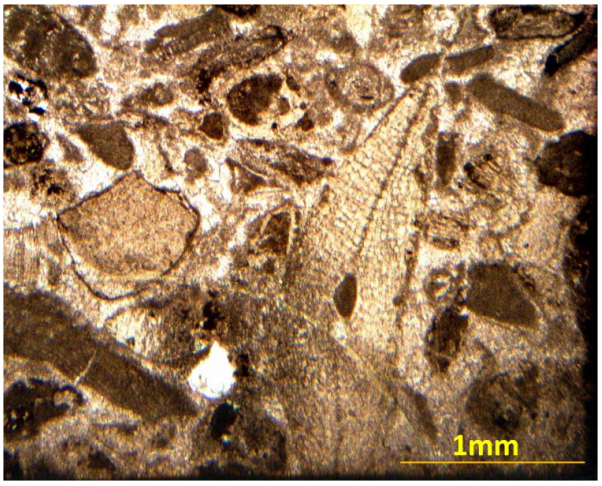

Plate 5.37 Thin section of Arip Cave Limestone at locality L10 under PPL showing poorly sorted biosparite with peloids and bioclasts.

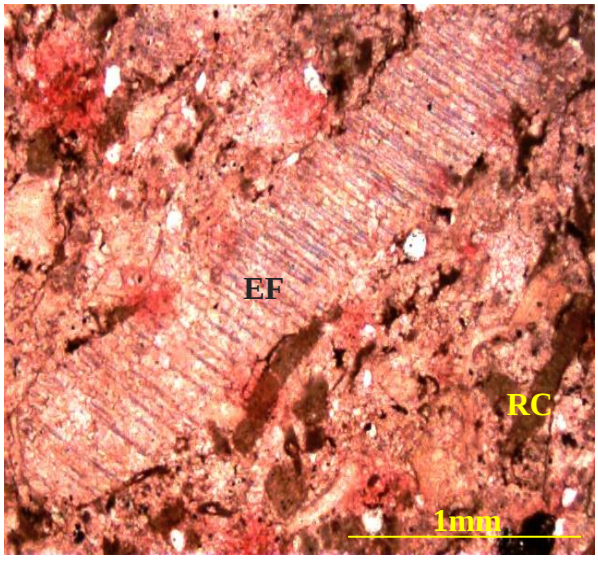

Plate 5.38 Thin section of Arip Cave Limestone at locality L10 stained with potassium ferricyanide showing micrite infilling rhodophyta chambers (RC). The echinoderm fragment (EF) is made up of sparry calcite.

Arip Valley Limestone

The rock is sparry calcite and micritic supported and not organically bound together during deposition. bioclasts form more than 60% of the rock and therefore it is classified as a wackestone (Dunham, 1962). It is composed of mainly micrite and some sparry calcite. It is classified as a biopelsparite according to the Folk (1952, 1962) as the rock contains very abundant sparry calcite with bioclasts and peloids.

The limestone is composed of about 30% calcitic mud, 45% fine grain sparry clacite and 2% quartz while bioclasts of mostly pelagic foraminifera form 20% of the limestone (Plate 5.39).

Details on the fossils has been discussed in the section on palaeontology (Chapter 4.3.3).

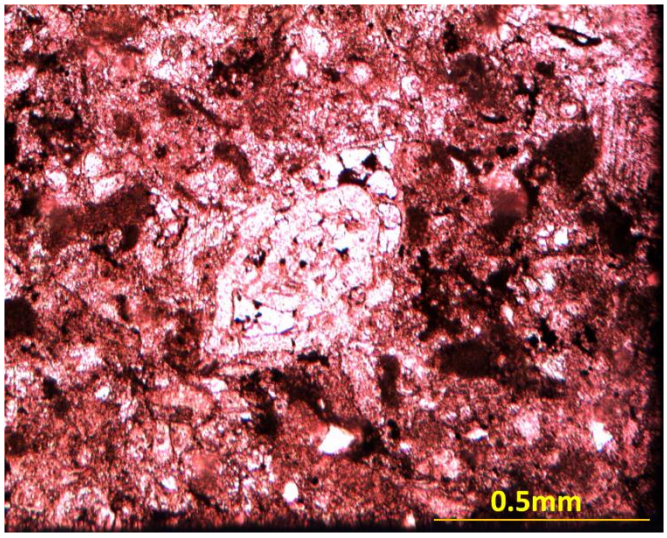

Plate 5.39 Stained thin section under PPL of Arip Nursery Limestone showing a fragmented foraminifera surrounded by micrite and sparry calcite with some angular quartz grains.

5.8 COAL PETROLOGY

Coal Petrology

Six coal samples were collected from the Ransi Member and a sample was taken from another part of the Tatau Formation in the Tatau area for coal analysis. Vitrinite reflectance (%Ro) determination was carried out on all the samples using oil immersion reflected light microscope to assist in interpreting the burial history of the coal bed in the Ransi Member (Plate 5.40; 5.41). It was also used for comparison with adjacent formations to determine relative stratigraphic positions.

The vitrinite reflectance (%Ro) of the Ransi Member ranges from 0.77% to 0.86% (Fig. 5.27(a-c)) while that of the coal in overlying Nyalau Formation in the Tatau area is between 0.4% to 0.65% (Pebrina , 2008). Only one sample was collected from the other part of the Tatau Formation which is poorly representated because of the lack of organic fragments present. It gave a value of 0.8%Ro (Fig. 5.27(a)). The vitrinite reflectance of the younger Balingian and Begrih Formations fall between 0.3% to 0.4% from a previous study (Wong, 2008). The older Belaga Formation has more than 1.5%Ro.

The approximate maximum depth of burial (Table 5.14) obtained from the vitrinite reflectance of the Belaga Formation is 3.41km which is deepest for the rocks in this area. The Ransi Member and other Tatau Formation coals were buried at a shallower depth of about 2.14km to 2.63km compared to the Belaga Formation. These results confirm the relative stratigraphic positions of the formations. The younger Nyalau Formation had an even shallower depth of burial of 0.87km to 1.80km compared to the Tatau Formation. The youngest Begrih and Balingian Formations were

buried at the shallowest depth of 0.32km to 0.87km. The Ransi Member has a similar range of Vitrinite Reflectance to the Tatau Formation sample confirming its position within the Tatau Formation.

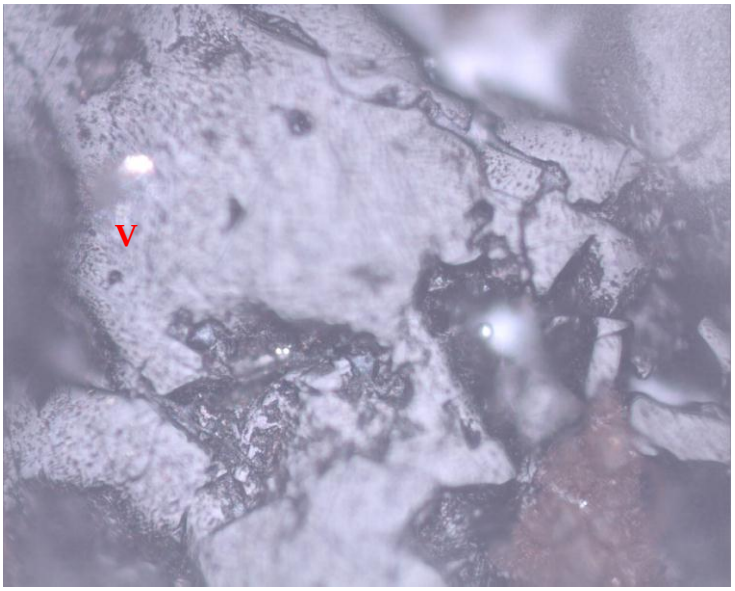

Plate 5.40 Polished section of coal (Vitrinite maceral) from locality L3, Hormat Pasifik Quarry of Ransi Member showingVitrinite.

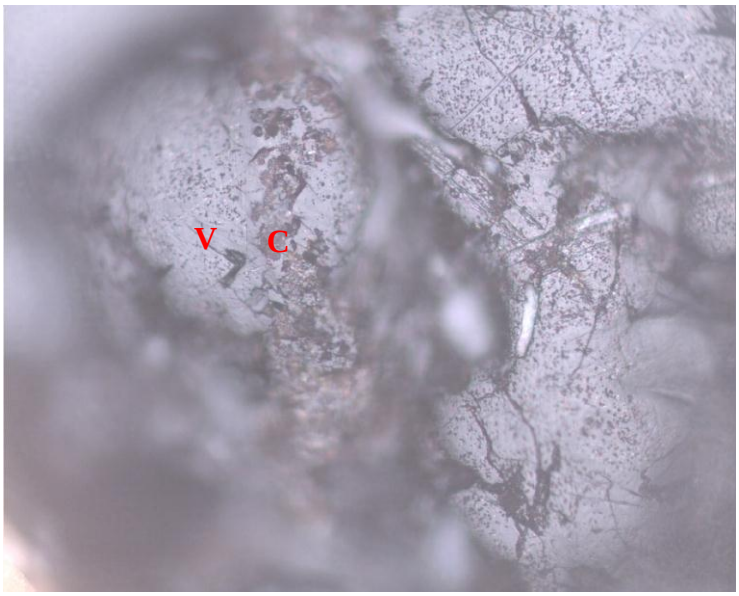

Plate 5.41 Polished section of L1, Tutong Hill of Ransi Member showing clay intercalated (C) with Vitrinite(V).

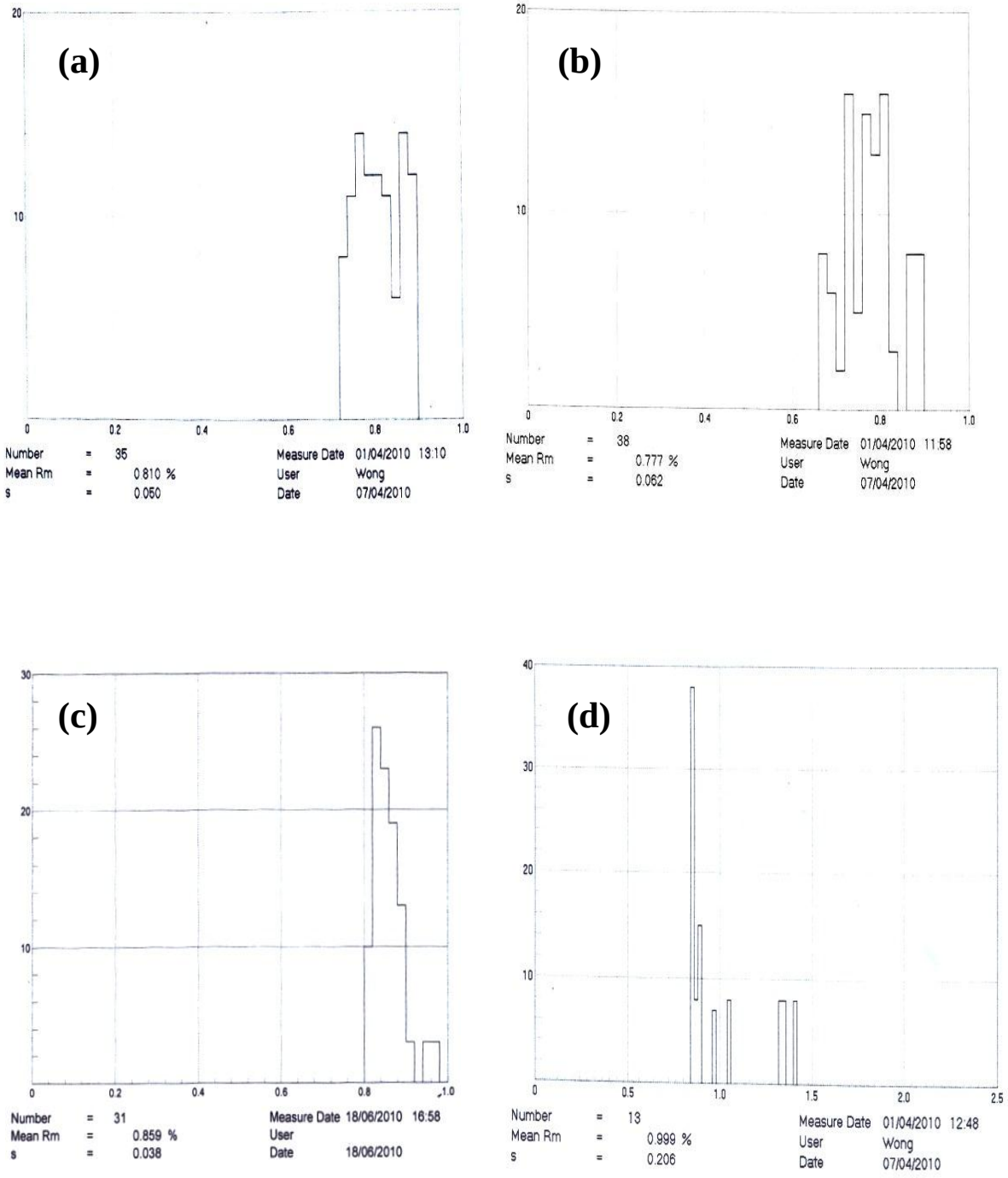

Fig.5.27 (a – c)Vitrinite reflectance (%Ro) of the Ransi Member. (d) Vitrinite reflectance (%Ro) of the Tatau Formation.

Formation	Vitrinite Reflectance (%R0)	coalification temperature (°C)	Estimated depth of burial (KM)
Balingian FM	**0.30** **0.40**	**38.4** **61.6**	**0.32** **0.87**
Nyalau FM	**0.40** **0.65**	**61.6** **100.7**	**0.87** **1.80**
Tatau FM **Ransi Member** **Other place**	 **0.78** **0.81** **0.86** **0.99**	 **115.0** **118.5** **123.2** **135.4**	 **2.14** **2.23** **2.34** **2.63**
Belaga FM	**1.50**	**168.2**	**3.41**

$$\text{Coalification temperature (°C)} = \frac{\text{In (\%Ro)} + 1.68}{0.124}$$

(After Barker & Pawlewicz, 1994)

Average thermal gradient of Southern Balingian Province (including inland Tatau area) is 42°C/km.

(After Shuntaro & Rosoul, 2005)

Table 5. 14 Mean vitrinite reflectance (%Ro) values of coal samples and estimated depth of burial (in km) for the different formations. Ransi Member has higher %Ro and higher depth of burial compare to Nyalau and Balingian Formations.

5.9 CONCLUSION:

The Ransi Member is composed of mainly conglomerate and coarse grained sandstone beds. Shale beds are rare and occur as thin beds or lenses between the sandstone beds. The Ransi Member sits unconformably above the Belaga Formation on top of the Eocene Unconformity (Fig. 4.1). This angular unconformity is clearly seen from the difference in the dips of more than 70° in the underlying beds and between 35° to 45° in the younger beds.

The lithology of the younger Ransi beds can also be easily distinguished from the underlying Bawang Member beds of the Belaga Formation. The underlying beds of Bawang Member consists of mainly dark grey shale interbedded with smaller numbers of thin sandstone beds. Some shale beds are whitish in color due to weathering. The rocks are highly deformed and tightly folded with high angles of dip and had undergone low grade metamorphism. Some of the shale had turn into slate. Normal grading is typical of the beds with well sorted sandstone fining upwards to shale in the turbiditic layers. Each bed starts with medium well sorted sandstone followed by convolute cross laminated sandstone and overlain by thick shale with parallel lamination. Complete Bouma sequences were not found in all the exposures (Fig. 4.4).

The angular unconformity was observed at two exposures at Ransi Hill (Fig. 4.39) and Tutong Hill (Fig. 4.43; 4.44). Based on the change in lithology of the lower beds and upper beds; it is suggested that the angular unconformity is located in between the two points. The angular unconformity is marked by an erosional surface on top of the tightly folded older Bawang Member beds. Overlying the angular unconformity are

the coarse grain conglomerate beds which can be clearly seen at Tutong Hill and Ransi Hill. The Ransi Member conglomerates sitting on top of the angular unconformity are probably the basal conglomerates of the Tatau Formation. The Ransi beds were deposited roughly parallel to the angular unconformity and dips from 30 ° to 50° towards the west or north. The dips are controlled by the palaeogeography and also the post depositional deformation affecting the different localities (Nichols, 1999).

The Ransi Hill exposure is probably the oldest part of the Ransi Member. The clasts are very coarse up to cobble size (Table 5.1). They range from sub-angular to sub-rounded in shape and the matrix is coarse sand. The beds fine upwards and are graded from clast supported conglomerate to pebbly sandstone upsection. The conglomerate beds at the bottom gradually transform into pebbly sandstone with less than 30% pebble content. The clasts composition of the conglomerate beds are generally of meta-quartzite, chert and some rhyolitic fragments. The metastable polymict conglomerate with clasts derived from various sources was transported and deposited at the edge of a continent. Some of the pebbly sandstone beds higher up in the section contain shallow marine burrows such as the *Ophiomorpha* (Fig. 4.33) suggesting the beds were deposited near the coast (Bann & Fielding, 2004). The rate of the sedimentation was rapid as can be seen from the poor sorting and sub-angular grain shapes and a wide range of clasts in the conglomerate beds.

The Hormat Pasifik exposure is a younger sequence than the Ransi Hill exposure as inferred from their relative positions in the maps. Most of the beds in this exposure are sandstone and a little bit of shale together with a thin coal seam. The grains in the sandstone were mainly made up of polycrystalline quartz and rock fragments such as

igneous and schist fragments. The grains are sub-angular to sub-rounded as the distance of the transportation from the source is relatively short. It suggests that the source of the polymict pebbly sandstone was derived mainly from the older low-grade metamorphic Belaga Formation. There is little primary clay present in the pebbly sandstone and siltstone beds. The vitrinite reflectance values suggest the coal had been buried deeper than those in the Nyalau Formation and upper parts of the Tatau Formation (Pebrina, 2008). The Ransi Member was deposited prior to the Nyalau Formation and is probably at the base of the Tatau Formation. The presence of less resistant clasts such as chert and quartzite in the beds and a coal seam together with thicker shale beds suggests the sediments were probably deposited in a lower swampy delta plain environment further down towards the coast compared to the conglomeratic deposits at Ransi Hill.

The Tatau Hill exposure is younger than that of the Hormat Pasific Quarry (Fig. 4.2) and is built up of stacked channel deposits (Fig. 4.50). Sandstone beds are dominant and shale is present only as thin lenses. The polymict sandstones are dominated by polycrystalline quartz and rock fragments. The petrology of the quartz grains is similar to those of the other exposures suggesting that the source was the same from an area or areas with low-grade metamorphic rocks and igneous rock similar to the Piring Hill rhyolite. Shale clasts and clay laminate are present but very rare in the sandstones indicating it is mature. The sub-angular to sub-rounded grains however indicate rapid deposition of normally graded beds suggesting that the sediment was deposited in relatively high energy and unconfined channels cutting across thin shale and carbonaceous beds not too far from the source (Tamura & Masula, 2003).

Tutong Hill is the youngest exposure of the Ransi Member in the area according to the strikes of the beds. It sits above the angular unconformity overlying tightly folded Bawang Member beds. It has within it abandoned channel deposits filled with dark shale (Fig. 4.45). The conglomerate beds are composed of polymict clasts such as quartz, chert and a few little granitic fragments. It suggests immature composition of the conglomerate. Sub-angular to sub-rounded clasts and the low matrix content of coarse-medium size sand indicate rapid deposition not too far from the source. The mixed composition of the both conglomerate and sandstone clasts suggest more than one source for the sediment. The petrographic properties of the quartz grains in the pebbly sandstone suggest they were derived from a low-grade metamorphic source. The igneous fragments found in the sandstone were similar with the rhyolite from Piring Hill. Therefore, the age of the Ransi Member should be younger than the Middle Eocene Piring rhyolite.

The Pelungau exposure is mainly formed of conglomerate beds with only some very thin shale lenses and thin fine sandstone beds. The conglomerate clasts range up to cobble in size and the clasts are mainly sandstone and shale fragments. This is an unstable conglomerate with less durable clasts. The clasts are well-rounded with clayey matrix suggesting poor sorting (Fig. 4.60). This polymict conglomerate suggests that the source of the clasts is of sedimentary origin and might be different from that of the Ransi Hill, Hormat Pasifik Quarry, Tatau Hill and Tutong Hill exposures. A synsedimentary fault was observed within the conglomerate bed (Fig. 4.58). This exposure was near to a major fault could have caused the conglomerate bed to be formed locally. Therefore, Pelungau conglomerate is not part of Ransi Member

Pelungau conglomerate beds might closely related to the young post-Miocene Anak-Nyalau fault which is much younger than Ransi Member.

The Ransi Member is mainly made up by conglomerate, sandstone and some thin shale beds. The overall sequence is fining upwards. Burrows are common in sandstone shale interbeds. The composition of grains in Ransi Member made up by quartz, chert and some lithic fragments. Compare to Nyalau Formation and other part of Tatau Formation. Ransi Member is more rudite, whereas Nyalau Formation is more arenaceous and Tatau Formation is dominated by argillaceous. The coal maceral analyses suggests that Ransi Member has similar depth of burial with Tatau Formation but is deeper than Nyalau Formation.

Diagenesis of the sandstone was observed under thin section. The sandstone samples from all of the Ransi Member outcrops show that the sandstone had undergone pressure solution with the presence of concavo-convex contacts (Plate 5.26). This feature is very common between the quartz grains. Pseudomatrix was also commonly observed from the samples (Plate 5.24). Quartz overgrowth (Plate 5.28) is significant in the samples suggesting that the depth of burial was probably deeper that 1000m before tectonic inversion (Morad et al., 2000). Shallow depth pressure solution diagenesis as a result of compaction was formed together with deep burial diagensis with quartz cementation and overgrowth suggesting the gradual change in diagenesis was related to post tectonic uplift. According to Morad et. al. (2000) quartz overgrowth and cementation only take place during late burial at temperatures between 142°C and 215°C (Fig. 5.28).

The diagenesis of the Arip Limestone is mainly in the form of recrystallization. This can be observed as cementation of bladed-prismatic calcite that grows directly on the bioclasts and calcite crystal surfaces (Plate 5.29).

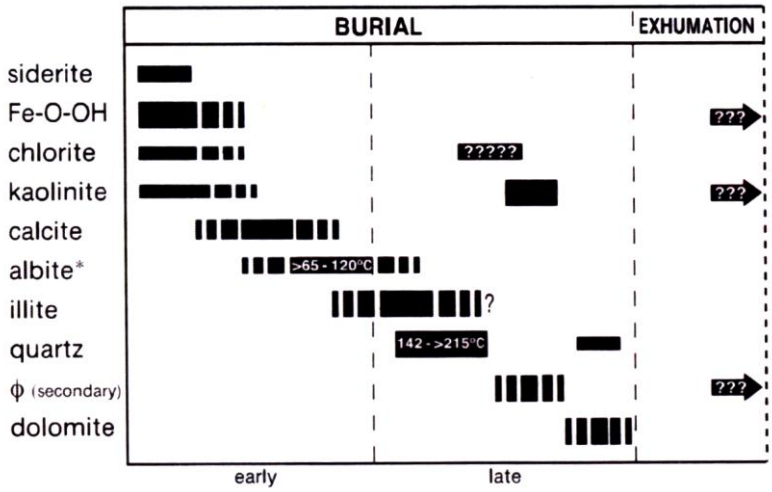

Fig. 5.28 Paragenesis based on textural evidence and geochemical consideration as proposed by Muad et al. (2000). Dashed bars indicate degree of uncertainty.

The graded conglomerate angular to sub-angular clasts up to 35 cm in the facies F1 at the lower section of Ransi Hill, Tutong Hill, Tatau Hill and Hormat Pasifik Quarry outcrops suggest a near source deposition. Whereas facies F2 of pebbly sandstone to medium grain sandstone in graded beds at the upper parts of the Ransi Member suggest longer distance of transportation with quartz, chert pebbles in the sandstone being generally sub-angular to sub-rounded. The presence of burrowing including *Orphiomorpha* and stratigraphical pinch outs suggest a lower delta plain depositional environment. Facies F3 with only thin shale lenses and abundant burrows is rare throughout the Ransi Member sequence and present in the upper sections. The deposition of the Ransi Member started high energy near source conglomeratic channel deposits that later changed into lower energy lower delta plain deposits with mainly sands and some pebbly sandstone deposited with richly burrowed sand-shale interbeds.